Nanoscale

Ion and Water Adsorption to Graphene and Graphene Oxide Surfaces

Journal:	*Nanoscale*
Manuscript ID	NR-MRV-05-2023-002452.R1
Article Type:	Minireview
Date Submitted by the Author:	31-Jul-2023
Complete List of Authors:	Carr, Amanda; Argonne National Laboratory, Chemical Sciences and Engineering Lee, Seung Eun; Argonne National Laboratory, Chemical Sciences and Engineering Uysal, Ahmet; Argonne National Laboratory, Chemical Sciences and Engineering

ARTICLE

Ion and Water Adsorption to Graphene and Graphene Oxide Surfaces

Received 00th January 20xx,
Accepted 00th January 20xx

DOI: 10.1039/x0xx00000x

Amanda J. Carr,[a]* Seung Eun Lee [a] and Ahmet Uysal [a]

Graphene and graphene oxide (GO) are two particularly promising nanomaterials for a range of applications including energy storage, catalysis, and separations. Understanding the nanoscale interactions between ions and water near graphene and GO surfaces is critical for advancing our fundamental knowledge of these systems and downstream application success. This minireview highlights the necessity of using surface-specific experimental probes and computational techniques to fully characterize these interfaces, including the nanomaterial, surrounding water, and any adsorbed ions, if present. Key experimental and simulation studies considering water and ion structures near both graphene and GO are discussed. The major findings are: water forms 1-3 hydration layers near graphene; ions adsorb electrostatically to graphene under an applied potential; the chemical and physical properties of GO vary considerably depending on the synthesis route; and these variations influence water and ion adsorption to GO. Lastly, we offer outlooks and perspectives for these research areas.

1. Introduction

Understanding ion organization near interfaces is fundamentally interesting to a range of applications including electrochemical energy storage, catalysis, corrosion, tribology, and separations among others.[1, 2] Two-dimensional carbon materials graphene and graphene oxide (GO) are especially promising for many of these applications. Graphene, made of sp^2 hybridized carbons, is one-atom thick and exists in two-dimensional flat sheets that can be cm large. It is conductive, transparent across nearly all wavelengths, and has an exceptional tensile strength. GO has both aromatic carbon regions and oxygen-based functional groups, the latter of which are usually introduced during synthesis. Consequently, GO is dispersible in water and polar solvents, and usually exists as two-dimensional flakes. Detailed information about graphene and GO syntheses can be found elsewhere.[3, 4] Combining graphene and GO in nanocomposite matrices provides additional advantages[5] that can be leveraged in, for example, biomedical[6, 7] and other sensors,[8] adsorption,[9, 10] and supercapacitor[11] applications. In particular, graphene and GO are excellent candidates for separation applications, including capacitive deionization, and filtration via ion sieving and/or adsorption. In these systems, ion and water interactions in the interfacial region formed between the passing liquid and graphene or GO surface govern application efficiency and effectiveness. Local concentrations, ion and water polarizations, and dynamics at these interfaces greatly differ compared to bulk properties. For example, the dielectric constant of bulk water is well known as $\varepsilon = 78$ but decreases to $\varepsilon < 20$ near interfaces.[12] The origin of this reduced dielectric constant is under debate and has been attributed to: unexpected alignment of water molecules near surfaces,[13] slower reorientation of water molecules in the interfacial region,[14] and a combination of excluded-volume effects and long-ranged anisotropic dipole correlations.[15] In another example, the local concentration of ions adsorbed to a surface can be orders of magnitude higher than the bulk concentration. Interfaces are self-organized microenvironments where molecules and water are confined to an asymmetric system.[16] Evidently, probing the interface directly is imperative toward understanding water and ion organization and behaviors.

Examining interfaces experimentally is challenging, as the interfacial region is significantly smaller, ~5 nm, versus the larger bulk, meaning many experiments are overwhelmed with bulk signal. Surface and interfacial techniques, including but not limited to microscopy, X-ray scattering, and interfacial spectroscopy, are especially critical for characterizing ion and water structures near graphene and GO. Full and detailed experimentally determined descriptions of graphene and GO surfaces, including information about the surface, water, and ions, are necessary. Arguably, this stipulation requires a combination of techniques to describe both the physical and chemical structures present in these systems. We will discuss some of these techniques as used to characterize ion and water organization near graphene and GO with an emphasis on multi-probe experiments.

Interface composition must be carefully considered with special attention paid to possible contamination. An interface consists of multiple components, i.e. a defined surface with media on either side (Figure 1). Creating a reproducible graphene or GO interface suitable to interfacial probes is not trivial, as will be discussed in detail later with examples of solid-liquid and air-liquid experiments. Substrates can influence

[a] Chemical Sciences and Engineering Division, Argonne National Laboratory, Lemont, IL 60439 USA
*Corresponding Author: carraj@anl.gov. 630-252-5258

water and ion behavior and may convolute experimental data. Media composition, such as humidity in air-liquid measurements and solvent purity in both air-liquid and solid-liquid measurements, may also vary and affect observations. Contamination, i.e. the unintentional or unintended introduction of additional species to the experiment, can greatly impact interfacial measurements, as many common ions and molecules present in air and liquids in small amounts are also surface-active. Detailed preparation information and experimental reproducibility are two strategies for understanding contamination versus true experimental results.

Computational techniques are especially informative for understanding ion and water organization near surfaces. In simulations, the interface can be examined directly, and molecular-scale details can be extracted. Cross validation with experimental data is important to ensure the simulation results reflect reality. Additionally, selecting comparable experimental techniques is necessary, as inferring interfacial information from bulk measurements can skew interpretation of computational results. Consolidating experimental and computational results is an effective strategy for probing surfaces and specific graphene and GO results will be discussed.

In this work, we highlight key experimental and computational results on water and ion organization near graphene and GO interfaces. We focus on interface-specific studies but will also mention bulk works that can provide surface information. A full characterization of a graphene or GO interface necessitates descriptions of the surface itself, the water, and any adsorbed ions, if present. External influences, including substrate and contamination effects, must also be considered. Notably, these stipulations are not necessarily unique to graphene and GO systems and implementing full, multi-probe analyses can have broad implications. These strategies and outlooks will pave the way toward understanding the fundamental science of water and ion behavior near both graphene and GO.

Figure 1. Summary of water and ion organization near graphene (left) and graphene oxide (right) interfaces. Examined samples have macroscale scale properties while water and ion structure near both graphene and graphene oxide require nanoscale investigations.

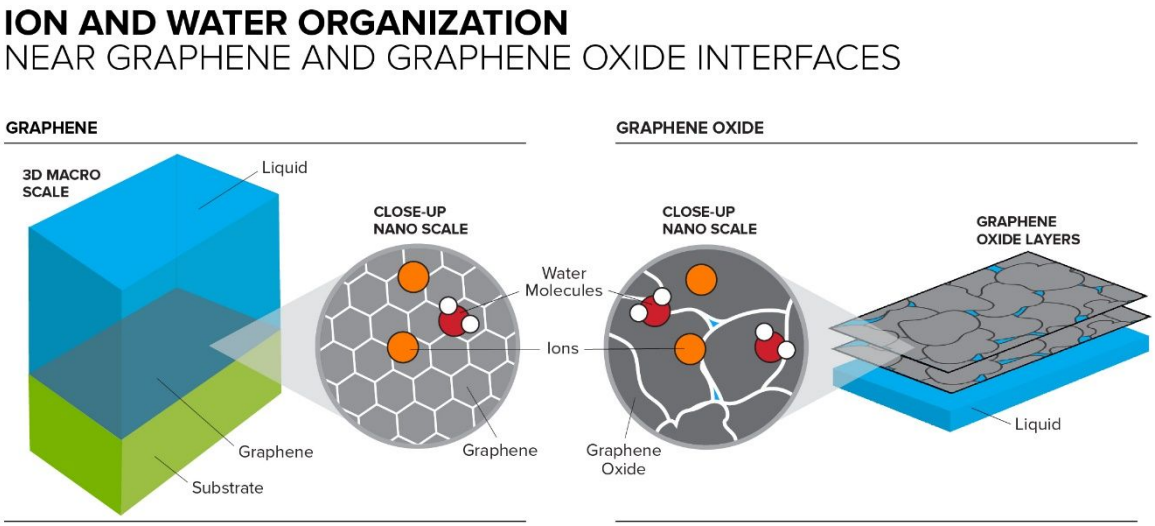

2. Interfacial Techniques

While a plethora of characterization techniques, including interfacial methods, exist, we will limit this discussion to common techniques used to understand ion adsorption and water organization near graphene and GO surfaces (Figure 2).

Synchrotron X-ray reflectivity (XR) is a powerful technique to determine interfacial structures.[17-20] Because the wavelength of X-ray light is comparable to atomic sizes and X-rays are scattered by electrons, X-rays can measure atomic-scale structures and reveal electron density information. Reflectivity experiments specifically measure the ratio of reflected and incident X-ray intensities *(R)* as a function of the angle between the incident beam and detector, 2θ, which is related to momentum transfer *Q* via $Q = 4\pi/\lambda \sin(2\theta/2)$ where λ is the X-ray wavelength. Informational about the electron density profile, ρ_e, near the surface is obtained by considering Q_z perpendicular to the sample and fitting the scattered intensities to

$$R(Q_z) = R_F \left| \frac{1}{\rho_e(z\to\infty)} \int \frac{d\rho_e}{dz} e^{iQ_z} dz \right|^2 \quad \#(1)$$

where R_F is the Fresnel reflectivity of an ideal mirror. Consequently, reflectivity is sensitive to changes in the electron density over *z* distances from the surface. XR is especially well-suited to probe buried interfaces, such as the solid-liquid interface formed between aqueous solutions and graphene surfaces (Figure 2A), because high energy X-rays can penetrate the bulk liquid without being absorbed. Notably, XR determines the *structure of an interface* and can provide chemical information if the electron densities of the species at the interface are significantly different, which can occur when ions are present. Measurements typically average signal over mm²

to cm^2 size spatial areas and can assess sample homogeneity by examining multiple spots.

Low-angle XR measurements can be completed on air-liquid[18] (Figure 2C) and solid-liquid interfaces and can be modelled by slabs with unique thickness, electron density, and roughness values via the Parratt formalism. Higher-resolution measurements, usually accessible at the solid-liquid interface because the surface roughness generated by capillary waves at liquid surfaces is too large to support high-angle data collection, can be modelled using calculated structure factors to describe the organization of scattering objects in reciprocal space. Neutron reflectivity (NR) follows similar principles using neutrons instead of X-rays, which are scattered based on the neutron scattering length density.[21] NR measurements can be sensitive to carbon and oxygen atoms via scattering contrast manipulation by doping common isotopes.

Resonant anomalous X-ray reflectivity (RAXR) measurements combine high-resolution XR with element specificity by measuring specular scattering at fixed *Q* values as a function of X-ray energy around the absorption edge of the targeted element (Figure 2B). Because the element-specific scattering, or anomalous dispersion, varies over the X-ray absorption edge, the detected scattering signal will show changes in amplitude and phase, which are related to the elemental coverage and distance from the surface, respectively.[22, 23] More complicated models to describe the location and distribution of resonant ions may be deployed to obtain additional details about atom locations and coverages. Consequently, RAXR is a *chemical* technique that reveals electron density information about a targeted element. Element choice is limited by the available X-ray energies, typically between approximately 10 – 100 keV at modern synchrotrons, depending largely on specific beamline optics.

Structural information about specific ions at the air-water and oil-waters interfaces can be obtained using X-ray fluorescence near total reflection (XFNTR) (Figure 2C).[18, 24, 25] In this technique, X-ray fluorescence intensity is measured as a function of *Q* around the critical angle, $Q_c = 4\sqrt{\pi r_e \Delta\rho}$, where r_e is the classical electron radius and $\Delta\rho$ is the difference in electron density at the interface of interest.[26] For systems at the air-water interface, Q_c ~ 0.022 Å^{-1}. Because the X-ray beam footprint is typically larger than the detector area, only the penetration depth of the incident X-ray varies over *Q*. Consequently, for $Q < Q_c$, collected fluorescence signal comes from ions in the interfacial region while signal collected at $Q > Q_c$ comes from ions at the interface and ions in the bulk. Using the known X-ray beam properties, the total illuminated volume can be calculated, and the number of adsorbed ions is determined directly. XFNTR is *chemically sensitive* because the X-ray fluorescence energy is element specific.

Microscopy methods, including transmission electron (TEM), scanning electron (SEM), and atomic force (AFM) are well known experimental probes that can provide *structural* information graphene and GO interfaces. Briefly, electron microscopy methods give high-resolution images of surfaces using an input steam of electrons. Structural features of a few nm in size can be resolved. Typical measurements are completed under vacuum although some liquid cells have been developed and deployed to examine graphene and GO with limited liquid resolution.[27] AFM is routinely used to characterize *ex situ* graphene and GO surfaces although liquid measurements are also possible. In particular, three-dimensional AFM can yield high-resolution information, approximately a few Å, about both the graphene and water structure at solid-liquid interfaces, described in detail by Garcia in a recent review.[28] Brewster angle microscopy (BAM) is an *in situ* technique used to image surfactants suspended on liquid surfaces that can provide *structural* information with μm lateral resolution.[29]

Vibrational sum frequency generation spectroscopy (SFG) is a nonlinear, interface-specific technique that can examine water organization near graphene, GO, and other surfaces (Figure 2C).[30, 31] SFG is inherently interfacial because it is a second-order optical process where the sum frequency signal created from two spatially and temporally overlapped photons only occurs when centrosymmetry is broken, a condition met by asymmetric interfaces. Data are collected using an incident visible light with intensity I_{vis} and an incident IR light with intensity I_{IR} as a function of IR wavenumber ω_{IR}. Measured SFG intensities are proportional to I_{vis} and I_{IR} and the magnitude of the effective non-linear susceptibility, $\chi^{(2)}_{eff}$, via

$$I_{SFG} \propto \left|\chi^{(2)}_{eff}\right|^2 I_{vis} I_{IR}. \#(2)$$

In the simplest approximation, resonant bands are modelled as *n* Lorentzian peaks within $\chi^{(2)}_{eff}$ via

$$\chi^{(2)}_{eff} \propto \left|\chi_{NR} + \sum_n \frac{A_n}{\omega_{IR} - \omega_n + i\Gamma_n} e^{i\phi}\right|^2 \#(3)$$

where χ_{NR} is the non-resonant signal contribution that is invariant to the IR wavenumber, φ is the phase between the non-resonant and resonant signal, A_n is the resonant peak amplitude, ω_n is the resonant peak wavenumber, and Γ_n is the dampening constant that determines peak width. Charged interfaces generate an electric field perpendicular to the surface, which induces additional signal contribution from farther into the bulk liquid, called the $\chi^{(3)}$ effect. When considering $\chi^{(3)}$explicitly, $\chi^{(2)}_{eff}$ becomes

$$\chi^{(2)}_{eff} \propto \left|\chi_{NR} + \sum_n \frac{A_n}{\omega_{IR} - \omega_n + i\Gamma_n} e^{i\phi_{2,n}} + \frac{\kappa}{\sqrt{\kappa^2 + \Delta k_z^2}} e^{i\phi_3} \chi^{(3)} \Phi_0\right|^2 \#(4)$$

where κ is the inverse Debye length, Δk_z is the inverse SFG coherence length, ϕ_2, and ϕ_3 are the phase angles for the $\chi^{(2)}$, and $\chi^{(3)}$ components, respectively, and Φ_0 is the surface potential. The SFG coherence length Δk_z is calculated using the experimental geometries[32] and ϕ_3 equals[32] $\tan^{-1}\left(\Delta k_z / \kappa\right)$. The remaining phase angle describes the interference between SFG signals.

Measurements frequently consider the vibrational water region from 3000 – 3800 cm^{-1}, as the measured intensities are sensitive to both the alignment and the number of interfacial water molecules. Generally, because the *magnitude* of $\chi^{(2)}_{eff}$ is

measured, background information about known molecular configurations and assumptions are necessary to obtain molecular orientation. Heterodyne or phase sensitive measurements can provide molecular orientation by measuring SFG signal against a local oscillator with a known phase, thus providing the real and imaginary contributions, $Re(\chi^{(2)})$ and $Im(\chi^{(2)})$, of $\chi^{(2)}_{eff}$ directly. Because ions adsorbed to the interface disrupt local water organization, which affects the measured SFG signal, the water region can also be used to indirectly detect adsorbed ions. However, the destructive interference of signal from different probe depths can make ion detection challenging. SFG provides *chemical* information and is well-suited to describe water structure and arrangement near interfaces. If the adsorbed ion has its own accessible vibrational mode, SFG can be used to directly probe adsorption.

Computational methods, including density functional theory (DFT) and molecular dynamics (MD), are powerful tools that can extract molecular-scale information and can examine targeted interfaces directly. DFT works typically calculate the electronic structures of ions and molecules and can be used to extract energetics associated with adsorption, binding, and bonding. *Ab initio* MD simulations calculate electronic structures and use them to understand molecular behavior, which is especially useful when examining covalent bond breaking and formation. These additional calculation makes *ab initio* MD more computationally expensive, meaning examined systems are usually smaller and have shorter timescales. Classical MD simulations approximate electronic structures using known force fields and can determine molecule movement and behavior including at targeted interfaces. Surface complexation modelling (SCM) is another computational method often applied to GO surfaces that uses bulk pH titration information to predict molecular adsorption. These methods are the most effective when verified or combined with experimental data.

Figure 2. Summary of some interfacial characterization techniques. A) Solid-liquid X-ray reflectivity.[2] Adapted with from ref [2] with permission from IOP Publishing, 2022. B) Resonant anomalous X-ray reflectivity.[23] Adapted from ref [23] with permission from Springer Nature, 2022. C) Liquid surface techniques including X-ray fluorescence near total reflection, X-ray reflectivity, and vibrational sum frequency generation spectroscopy.[1] Adapted with permission from ref [1]. Copyright 2022, American Chemical Society.

3. Graphene Surfaces

3.1 Water organization: Structural Analyses

Experimentally characterizing ion and water structure near graphene requires directly probing the nm-sized interfacial region between the aqueous liquid and solid graphene. Such experiments are challenging because measured intensities are usually dominated by the bulk solution, which behaves differently than the interfacial solution. Interface-specific techniques are then necessary to observe and understand ion and water organization.

An early high-resolution XR work probed water organization near epitaxial graphene on silicon carbide and observed via XR works where the epitaxial graphene coverage was more complete.[2, 34] In ref [34], combining high-resolution XR data (Figure 3A), modelled electron densities (Figure 3B) and detailed MD simulations (Figure 3C) revealed that most water molecules lay parallel to a graphene surface but some water molecules may orient away from the graphene, i.e. with their hydrogen atoms facing 60° ≤ θ < 90° with respect to the surface (Figure 3D).[34] This organization supports non-symmetric water polarization near the graphene surface. Notably, all of these XR studies reported: a non-trivial, low-density gap about 1 Å thick, after considering the radii of both the carbon atoms of graphene and molecular water, between the water and pristine graphene; and 1-3 hydration layers with an interlayer spacing of

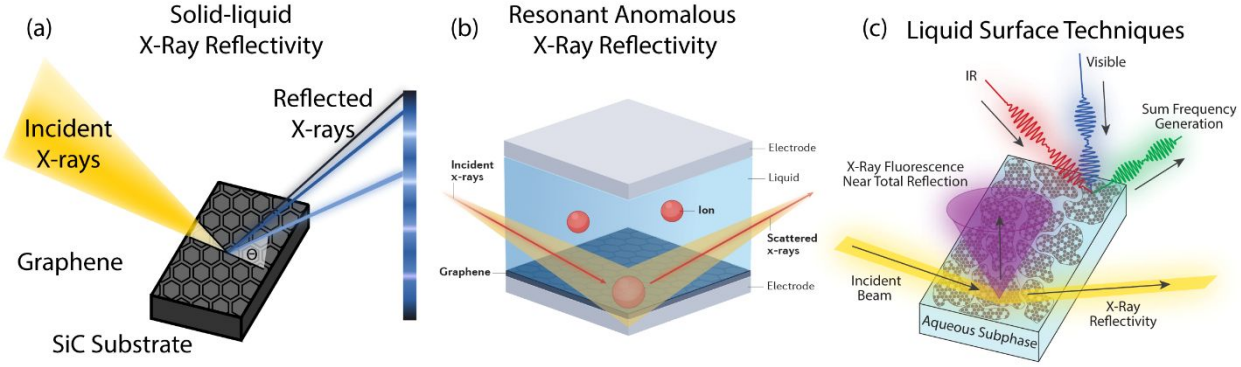

detailed model fits that water organization changes based on the composition of the surface.[33] For multilayer graphene samples with variable surface coverage, water may organize differently near the buffer layer grown between the epitaxial substrate and first layer of graphene compared to pristine graphene. XR cannot directly probe water orientation or chemical interactions. Instead, supporting classical and *ab initio* MD simulations demonstrated stronger interactions between water and this buffer layer versus water and graphene, likely due to oxygen functional groups present on the buffer layer. This substrate effect was less noticeable in later high-resolution 3 Å, which were attributed to distinct water populations for each layer of graphene.

Microscopy methods can also yield interfacial structural information at the water-graphene interface although obtaining molecular-scale resolution is challenging. Early electron microscopy works demonstrated imaging of water inside carbon nanotubes via TEM[35] and nanoconfined water sandwiched between two layers of graphene.[36] However, electron microscopy typically cannot yield molecular-scale information about the liquid phase and has not been sufficient to characterize water layering.[28] High-resolution atomic force

microscopy (AFM) can provide molecular-scale information about solid-liquid interfaces[37] and three-dimensional AFM works have detailed water structure near graphene, as covered in detail elsewhere.[28] Briefly, a three-dimensional AFM work on pristine graphite[38] demonstrated water layering with an interspace distance of 3 Å, in good agreement with prior high-resolution XR studies.[2, 33, 34] Validation across experimental methods is critical for establishing fundamental knowledge of these interfaces. Other three-dimensional AFM studies have observed significant airborne hydrocarbon contamination for graphene samples submerged in water.[28] These species can be introduced by exposing the liquid water or graphene to the atmosphere for even a few seconds and can strongly impact nanoscale, e.g. water layering and interfacial dielectric constant, and macroscale, e.g. flow behavior and hydrophobicity, properties.[28] Evidently, understanding contamination is imperative for reconciling differences in experimental data. Experimental methods that provide chemical information can be useful to distinguish contamination at the graphene-water interface from other components, as will be discussed in detail later.

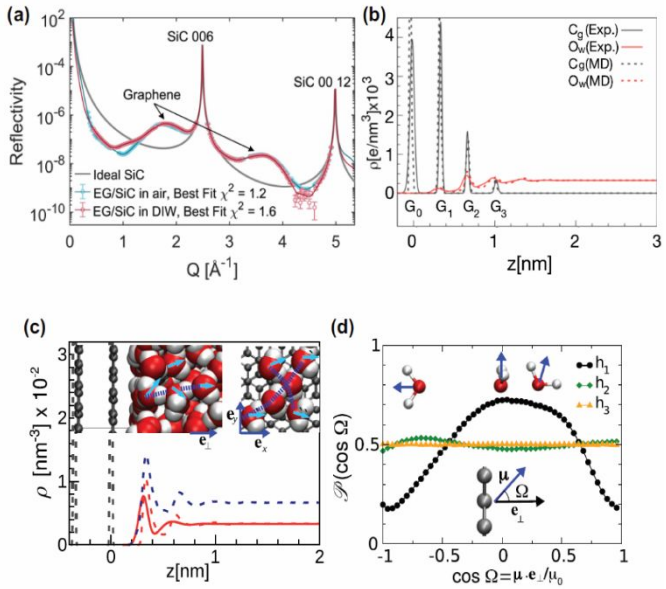

Figure 3. A) Measured high-resolution X-ray reflectivity data of multilayer epitaxial graphene (EG) on its native SiC substrate in air and water. B) Electron density profiles derived from best-fitted models of high-resolution X-ray reflectivity data of multilayer epitaxial graphene in water and molecular dynamic (MD) simulations. C) Comparison of experimental (solid red line) and MD simulations (dashed lines)-derived water density profiles of monolayer epitaxial graphene in water. The inset shows MD simulation snapshots of the water-graphene interface along the surface normal direction (left) and in the plan within $z < 0.5$ nm (right) where the arrows show the water dipole moments, and the dashed lines indicate hydrogen bonds. D) Water orientation probability distribution functions within different water regions: $h_1 = 0 < z < 0.5$ nm, $h_2 = 0.5$ nm $< z < 1$ nm, and $h_3 = 1$ nm $< z < 1.5$ nm. In these distributions, the water orientation is given by *cos(Ω)* where *Ω* is the angle between a water dipole moment and a unitary vector normal to the graphene surface.[34] These figures have been adapted from ref [34] under the terms of the Creative Commons Attribute 4.0 International License.

3. 2 Water Organization: Chemical Analyses

A full understanding of the graphene-water interface necessitates additional chemical information and a comprehension of water molecule orientation with respect to graphene. A highly ordered water population near graphene was detected with SFG using CVD graphene transferred to an optically transparent sapphire support.[39] Montenegro et al. then probed water organization near monolayer CVD graphene transferred to a transparent CaF_2 window under various applied potentials using SFG.[40] They observed an asymmetric response in water organization as a function of the applied voltage where the typical two water bands indicative of H-bonded water were present at positive voltages but disappear for negative voltages. At negative voltages, a sharp blue-shifted signal appears that is usually indicative of a dangling OH bond, i.e. a hydroxide bond pointing out of the surface that is unable to form hydrogen bonds. It is important to note that typical SFG experiments measure the *magnitude* of the second-order nonlinear response, $\left|\chi_{eff}^{(2)}\right|^2$, meaning molecular orientation information is lost. Nonetheless, Montenegro et al. deconvoluted the measured SFG intensity into $Re\left(\chi_{eff}^{(2)}\right)$ and $Im\left(\chi_{eff}^{(2)}\right)$, the latter of which can provide molecular orientation. They assigned the blue-shifted sharp spectral feature present at negative voltages to hydroxide bonds from water that are pointing up toward the graphene and assigned the signs of the remaining SFG signal based on reports of the free air-water[41] and air-surfactant-water interfaces.[41-43] Their assignments imply the remaining SFG signal across all voltages comes from water molecules facing down toward the bulk, meaning that even when the graphene surface is negative, the partially positive hydrogen atoms of water face away from graphene. Such an assignment contrasted with SFG spectra calculated via MD simulations, published a year prior.[44] In another report, Montenegro et al. extracted additional molecular orientation information about this dangling hydroxide using the same methods.[45]

In a responding work that was also highlighted in a comment,[46] Wang et al.[47] used heterodyne SFG to examine water organization near graphene under applied potentials (Figure 4A). In heterodyne measurements, the phase of the generated SFG signal is measured explicitly and $Im\left(\chi_{eff}^{(2)}\right)$ is probed directly. Their voltage-dependent measurements show that interfacial water faces up toward the graphene when a negative voltage is applied and down toward the bulk water when a positive voltage is applied, as expected and in direct contrast to Montenegro et al. Wang et al. additionally argued that blue shifted sharp feature assigned to a dangling OH bond must be from Ca-OH species existing on the CaF_2 window due to hydroxylation. The authors support this argument by measuring additional data at high pH, which are identical to SFG data measured at negative potentials (Figure 4B-E), and by calculating the true surface charge of the CaF_2-graphene interface from their SFG data. The total CaF_2-graphene surface charge does not match the graphene surface charge probed via Raman spectroscopy, meaning the CaF_2 must undergo a pseudocapacitive process and influence SFG intensity (Figure 4F). Prior SFG papers noted the likely presence of water on either side of graphene on a CaF_2 substrate[48] and the reactivity of CaF_2 over pH[49, 50] and discussed the possible effects of the substrate on SFG signal.

Taken together, these reports highlight the importance of characterizing and considering all components of the interface and the challenges associated with preparing reproducible graphene samples. While computational efforts have suggested SFG observation of a dangling water hydroxide,[44] chemistry occurring at the CaF_2 support window has largely obscured this signal.[46, 47] Such interactions with the CaF_2 window were possible because of excess water introduced during transfer of the CVD graphene from its native copper growth material to the optical window. Other reports have noted the persistence of intercalated water on graphene as well as the effects of the underlying substrate on measured graphene properties, most notably wettability as assessed via water contact angle.[51] Similarly, creating consistent graphene samples is not trivial. For example, an earlier SFG work of CVD graphene transferred to a CaF_2 window reported noisy signal and minor changes in intensity over applied potential but stated that sample variation prevented definitive conclusions.[48] Providing full experimental details and considering sample variation are critical for interpreting results across reports and understanding fundamental water behavior.

While most research efforts have focused on the graphene-water and substrate-graphene interfaces, it is also possible to suspend graphene at the air-water[52-54] and oil-water interfaces.[55] In these examples, two-dimensional graphene particles of different shapes were obtained by photolithography etching CVD graphene. The graphene particles were then transferred to either an air-water or oil-water water and characterized primarily with interference reflection microscopy.[55] Creating graphene particles enabled examination of a true two-dimensional colloid system and these reports investigated interparticle interactions, particle dynamics, and aggregation.

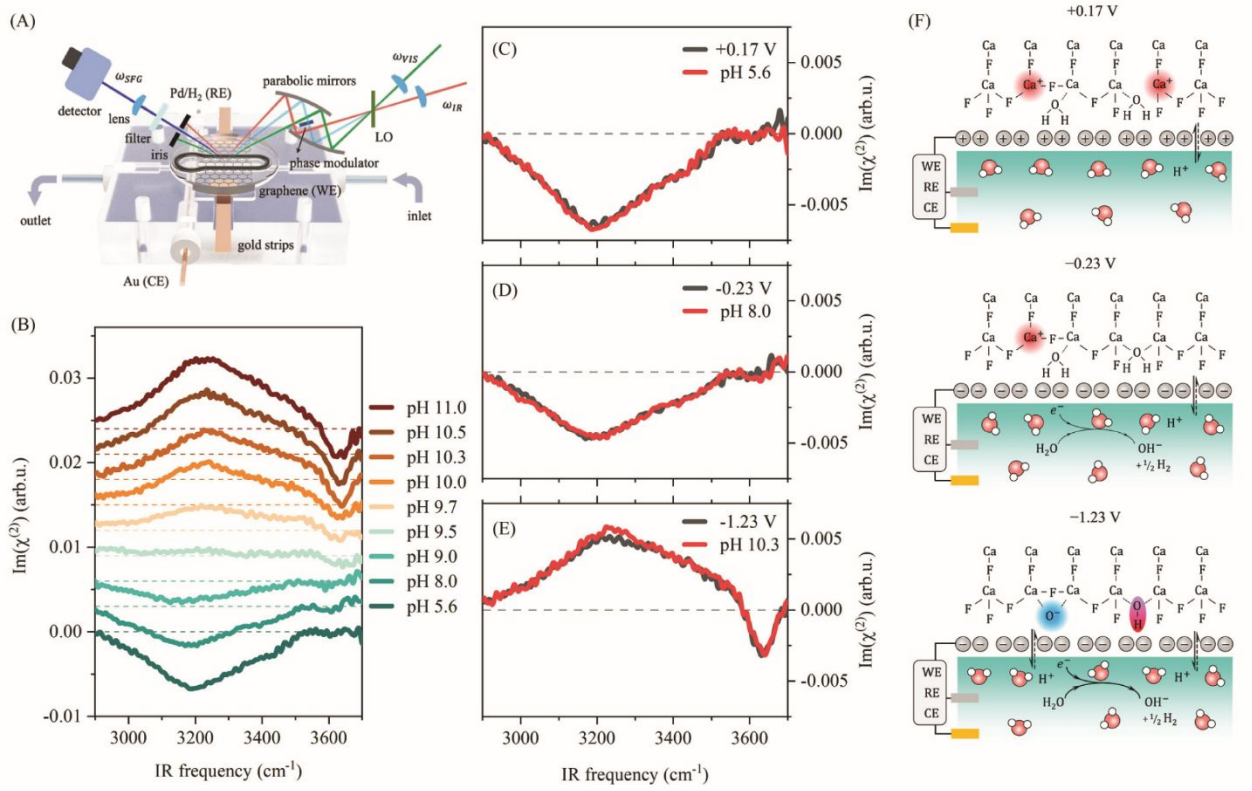

Figure 4. A) Experimental setup of an *in situ* electrochemical cell for heterodyne vibrational sum frequency generation spectroscopy measurements of graphene on a CaF_2 support. B) Hydroxide stretching $Im(\chi^{(2)})$ spectra at the CaF_2-supported graphene-water interface at different subphase pH values. C-E) Comparison of applied voltage and subphase pH on hydroxide $Im(\chi^{(2)})$ spectra. F) Schematic of the CaF_2-supported graphene-water interface in a 1 mM $NaClO_4$ solution. At +0.17 V, no chemical reactions occur at the graphene-water interface and the CaF_2 window has a positive charge. At -0.23 V, hydrogen evolution via water splitting begins, and hydroxide ions accumulate at the graphene-water interface, which increases the local pH and reduces the CaF_2 surface charge. At -1.23 V, excess hydroxide ions favor the hydroxylation of the CaF_2 window to create Ca-O-H bonds.[47] These figures have been adapted from ref [47] under the terms of the Creative Commons CC BY license.

3.3 Ion Adsorption and Influence on Water Organization: Structural Analyses

Determining molecular-scale, interfacial information in graphene systems containing additional ions under applied potential is more complicated. Typically, ideal monovalent ions will form an electrical double layer (EDL) near a charged surface where one type of ion adsorbs to the surface and the counterion co-adsorbs farther away in alternating layers, as described in the Poisson-Boltzmann equation via an exponential decay charge distribution.[56] Indeed, the EDL formed for model ions near a substrate has been observed experimentally with X-ray standing waves,[57] an interfacial X-ray fluorescence technique, matches this model. These simple models cannot accurately describe the behavior of multivalent ions, which can induce counterion adsorption, complex ion organization within the diffuse layer, and charge reversal with respect to original surface. Such EDL complexity has been documented for nearly

40 years.[56] Early computational works predicted surface charge amplification or overcharging for ions adsorbed to graphene[56] and speculated that adsorbed water influenced overcharging,[58] both of which will be discussed in detail later. Graphene is a particularly advantageous surface to examine overcharging because it is both conductive and lacks functional groups, meaning the surface charge can be manipulated. These features also mean observations on other surfaces may not apply to behavior near graphene.

Probing these ion distributions and water behavior near graphene necessitates clean, contamination-free surfaces. A low angle XR work on CVD graphene in air and water revealed contamination on the graphene surface,[59] likely residual from the CVD transfer process as fully removing polymer support layers from CVD graphene after transfer is extremely challenging.[60] Additional XR data for graphene in phosphate buffer saline hinted at ion adsorption but was not conclusive because of the contamination. AFM measurements in air and water confirmed sample defects and contamination signal.

Recently, our group deployed high-resolution XR and RAXR (Figure 5A-F) to characterize the organization of water and trivalent ion Y^{3+} near a charged graphene surface via electron density profiles (Figure 5G).[2] The combination of using epitaxial graphene on its native SiC substrate, cleaned and inherently free from contaminates, and a higher X-ray energy allowed high-resolution data collection, with a Q_{Max} ~ 5.5 $Å^{-1}$. This improved resolution facilitated detailed interfacial structure analysis. XR analysis revealed a distinct layer of water adsorbed about 2.8 Å away from the graphene without ions present. When Y^{3+} is in solution, two unique adsorbed populations are observed about 2.3 Å and 4.9 Å away from the graphene surface. These signals are assigned to two layers of organized interfacial water based on the measured no ion case and previous high-resolution XR reports on graphene in water without an applied potential.[33, 34]

RAXR measurements on graphene showed a diffuse profile of adsorbed Y^{3+} with unexpected high coverage, indicative of cation overcharging.[2] Specifically, RAXR measurements revealed 1 adsorbed Y^{3+} per 11.4 ± 1.6 $Å^2$ while the calculated capacitance determined from cyclic voltammetry (CV) predicted 1 adsorbed Y^{3+} per approximately 240 $Å^2$. This difference is attributed to the difficulty of probing metal ions without interference from their counterions electrochemically, as CV measures the total charge of the system and cannot easily decouple the absolute number of adsorbed cations and anions. In contrast, RAXR examines the targeted cation directly and is not influenced by counterion co-adsorption.

Figure 5. A-F) Resonant anomalous X-ray reflectivity data for epitaxial graphene on a SiC substrate in 10 mM YCl_3 solution held at -0.5 V. Panels show scattering data collected as a function of incoming beam energy varied around the *K*-edge of yttrium at different momentum transfer values. G) Total electron density profile derived from modelled high-

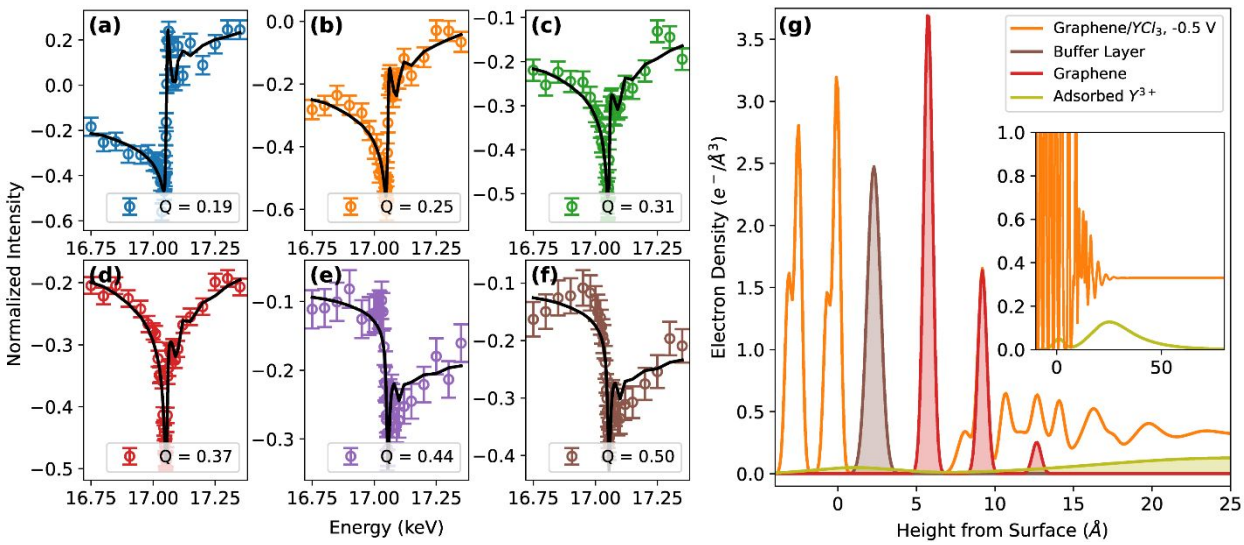

resolution X-ray reflectivity data (orange line) and yttrium-specific electron density profile derived from fitted resonant anomalous X-ray reflectivity data (yellow line).[2] These figures have been adapted from ref [2] with permission from IOP Publishing, 2022.

3.4 Ion Adsorption and Influence on Water Organization: Chemical Analyses

Additional chemical information is necessary to understand the role of water near graphene while ions are present. McCaffrey et al. utilized second harmonic generation (SHG), a non-linear, interfacial technique that is actually a special case of SFG, to probe NaSCN adsorption to multilayer graphene as a function of subphase concentration.[61] After correlating the measured SHG intensity to the number of adsorbed ions, the authors determined the free energy of SCN^- ion adsorption to the graphene as -8.5 ± 1.1 kJ-mol, a value that is strikingly similar to the free energy of SCN^- ion adsorption to the air-water interface, -6.78 ± 0.3 kJ-mol. Supporting MD simulations showed that ion adsorption to graphene is fundamentally different compared to adsorption to the free air-water interface even though the adsorption energies are similar. They speculate adsorption to graphene is enthalpically driven by favorable interactions between the graphene and ion.

Recently, Yang et al. used SFG to probe bilayer graphene floating on dilute salt solutions of Na_2SO_4, $(NH_4)_2SO_4$, and NH_4Cl at different applied potentials.[62] Measurements at the open circuit potential showed an increase in SFG intensity in the

water region over subphase Na_2SO_4 (Figure 6A) and $(NH_4)_2SO_4$ (Figure 6B) concentration, interpreted as an accumulation of SO_4^{2-} ions at the surface although the driving force for this sulfate adsorption is unclear. These data also showed a prominent dangling hydroxide signal at 3700 cm^{-1}, attributed to water molecules near the graphene. As discussed in detail previously, it is possible this signal is from water trapped between the two layers of graphene, as the signal does not vary over subphase concentration or composition. Such signal also does not change monotonically over positive (Figure 6C, E) or negative (Figure 6D, F) applied potential for Na_2SO_4 or $(NH_4)_2SO_4$, as predicted by a computational work on the plain graphene-water interface.[44] Positive applied potentials increase the measured SFG intensities, likely due to enhanced water molecule alignment from the applied electric field. Negative potentials also changed the intensities of the peaks but the trend over voltage is not obvious. Notably, the dangling OH signal, typically appearing at 3700 cm^{-1}, red-shifts and changes in intensity for negative potentials. Additional experiments are needed to understand the overall behavior and nature of water and ion organization especially for graphene under applied potentials.

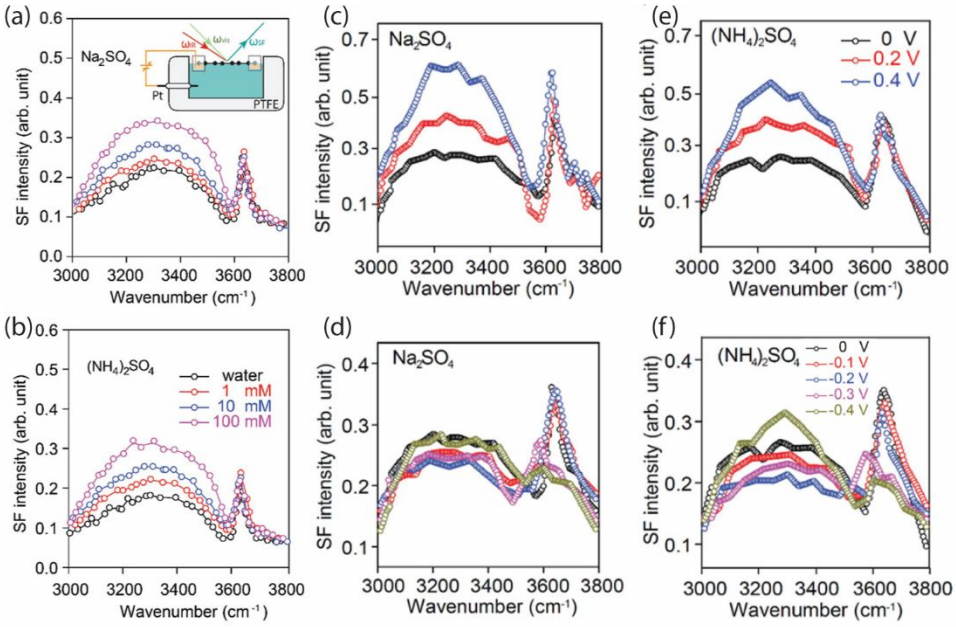

Figure 6. A) Vibrational sum frequency generation spectroscopy (SFG) data of the hydroxide stretch region at open circuit potential for graphene contacted with water (black), 1 mM (red), 10 mM (blue), and 100 mM (purple) Na_2SO_4. Inset shows *in situ* electrochemical cell where graphene floats on the subphase. B) SFG data at open circuit potential for graphene contacted with water (black), 1 mM (red), 10 mM (blue), and 100 mM (purple) $(NH_4)_2SO_4$. Panels A and B share the same legend. C) SFG data at 0 V (black), 0.2 V (red), and 0.4 V (blue) for graphene contacted with 10 mM Na_2SO_4. D) SFG data at 0 V (black), -0.1 V (red), -0.2 V (blue), -0.3 V (purple), and -0.4 V (yellow) for graphene contacted with 10 mM Na_2SO_4. E) SFG data at 0 V (black), 0.2 V (red), and 0.4 V (blue) for graphene contacted with 10 mM $(NH_4)_2SO_4$. F) SFG data at 0 V (black), -0.1 V (red), -0.2 V (blue), -0.3 V (purple), and -0.4 V (yellow) for graphene contacted with 10 mM $(NH_4)_2SO_4$. Panels C and E share a legend, and panels D and F share a legend.[62] These figures have been adapted from ref [62] under the terms of the Creative Commons CC BY 4.0 license.

Given the experimental challenges of creating high-quality graphene samples and isolating true sample signal, computational efforts to understand water structure and ion adsorption to graphene can be beneficial. We note that we have limited this discussion specifically to works considering water and ion behavior near graphene surfaces. Indeed, there are many additional works on complicated EDL structures near charged surfaces with different multivalent ions, including more recent reviews.[63, 64]

As mentioned previously, early computational works observed complicated EDL structures for ions near planar surfaces, including graphene. Jiménez-Ángeles and Lozada-Cassou[56] first reported an accumulation of ions near a similarly-charged surface and described this phenomenon as a unique case of "overcharging" separate from classical "charge reversal"

and "charge inversion." In "charge reversal," the magnitude of ions adsorbed to an oppositely charged surface is greater than the original surface charge. These additional ions cause the total electric field direction to reverse. Counterions with the same charge as the original surface may then adsorb near these ions, which is called "charge inversion." Overcharging is a specific subsection of complicated charge reversal and charge inversion. The authors[56] attributed overcharging and complicated charge reversal and charge layering effects to both electrostatics and excluded volume where excluded volumes of larger particles enhanced adsorption and overcharging. Another report[58] deployed MD simulations to understand the impacts of water and complex ion adsorption on overcharging, which they refer to as "surface charge amplification." They argued overcharging can occur because water molecules are preferentially adsorbed onto the charged surface instead of the hydrated ions. This water layer is aligned such that the average molecular dipole is enhanced, which promotes ion and counterion adsorption.

In a more recent work, Jiménez-Ángeles et al.[34] examined the interaction energy between ions near a graphene surface using MD simulations that specifically considered ion-ion interactions and compared the results to experimental, high-resolution XR data on graphene in water, as discussed in a previous section. Their computational work showed an asymmetric water polarization field around ions < 1 nm away from graphene for positively and negatively charged ions with the same ionic radius. Notably, for the cation, the polarization field in the *z* direction is reversed near the graphene surface. For the anion, the polarization field is parallel to the graphene surface. They attribute this effect to the asymmetric polarization of water and note that simplistic image charge models cannot capture this behavior. The authors also observed asymmetric water polarization for two oppositely charged ions near a graphene surface, which affects ion-ion interactions.

Son and Wang[65] investigated the impact of interfacial water on ion adsorption to graphene using MD simulations by independently controlling the polarization of the ions, solvent, and surfaces. They deployed image charge interactions to model the difference in polarization between the solvent and surface, an exact solution where an identical particle with opposite charge is placed beyond the boundary condition to invoke attraction or repulsion to the boundary. Careful investigations using different molecular force fields, graphene-water and vacuum-water interfaces, revealed that the image charge interactions of water strongly influence ion adsorption to charge neutral interfaces. If the image charges of the surrounding water are excluded, more ions adsorb to the graphene-water interface compared to the vacuum-water interface, which is consistent with classical continuum electrostatics predictions and contrary to the experimental results by McCaffrey et al., which show similar adsorption energies for ions at the graphene-water interface and ions at the air-water interface.[61] When these image charge interactions are included, they significantly reduce ion attraction to the graphene-water interface such that ion adsorption is nearly identical to the vacuum-water interface. They posit this cancellation stems from the asymmetric solvation of water molecules at the interface. Notably, when a potential is applied, the graphene-water surface shows more charge separation versus the vacuum-water interface. Additional calculations show this charge separation is likely caused by "lowering the electrostatic energy of the system dipole."[65]

In a similar vein, there is considerable interest in understanding ionic liquid (IL) organization near graphene surfaces, as these systems are directly applicable to energy storage research.[66] While a detailed discussion of IL organization at graphene surfaces is beyond the scope of the current paper, we note that others have examined IL-graphene systems experimentally[67-70] and computationally[71, 72] in order to better understand molecular ordering near a charged surface. In these very concentrated systems, a clear EDL is not formed. Instead, ions organize into multiple ionic layers, which can result in "overscreening" of the original surface charge,[73] a scenario similar to overcharging described previously.

4. Graphene Oxide Surfaces

4.1 Graphene Oxide as an Amphiphile

Water organization near graphene oxide (GO) is considerably more complicated compared to organization near graphene. First, unlike graphene, GO is not composed only of perfect sp^2 hybridized carbons. Rather, there are additional functional groups, typically hydroxides, epoxides, and carboxylic acids, and hydrogen-terminated carbon atoms throughout. Consequently, GO has both hydrophobic and hydrophilic domains. It is important to note that there is no universal GO chemical structure. The location, density, and types of functional groups present on GO strongly depend on the chosen synthetic method and purification steps.[74, 75] Efforts are currently being made to standardize GO characterization across synthesis methods.[76] Second, GO can have a strong intrinsic charge because its functional groups may deprotonate/protonate depending on the aqueous conditions. Naturally, the magnitude of this charge also depends on the specific GO structure. Third, because GO is typically created via exfoliation of graphite, GO primarily exists as two-dimensional flakes, which can vary significantly in size from nm to µm. This physical structure directly contrasts with planar graphene and necessitates additional consideration of the flake edges. The hydrophilic functional groups of GO greatly improve its solubility in polar solvents, a marked difference compared to hydrophobic graphene.

Cote et al. were the first to suspend 2D GO flakes isolated from graphite on water in 2009, which they called "graphite oxide single layers" to distinguish from general bulk "graphite oxide."[77] The authors predicted GO surface activity by considering GO as an amphiphile and were able to float GO flakes on water via Langmuir deposition, where they suspended isolated GO in a volatile organic solvent and added the suspension drop-by-drop on top of water in a Langmuir trough. After solvent evaporation, the trough barrier pushed the GO flakes together into a film. SEM and AFM images of GO flakes transferred to silica wafers at different points during the

compression process revealed irregularly shaped GO flakes that moved toward each other and eventually touch at the flake edges to create a cohesive, smooth film. Additional compression created many overlapping flakes with additional wrinkles and folds.

In a follow up work, the same group investigated GO behavior at air-water, oil-water, and water-solid interfaces (Figure 7).[78] They found GO flakes can rise through the aqueous subphase and become pinned at the air-water interface if given enough time. This process can be sped up by adding carbon dioxide bubbles to the subphase (Figure 7B-C), to which the GO flakes are attracted, as confirmed with *in situ* BAM images of the liquid surface (Figure 7D-E). *Ex situ* SEM images of GO flakes on solid substrates showed an accumulation of larger GO flakes at the liquid surface while smaller flakes remained in the subphase, consistent with an overall change in flake hydrophilicity depending on the size, as flake edges tend to be more hydrophilic. GO flakes can also act as emulsifiers by stabilizing the oil-water interface and can improve the solubility of other nanomaterials, such as carbon nanotubes, in aqueous solutions.

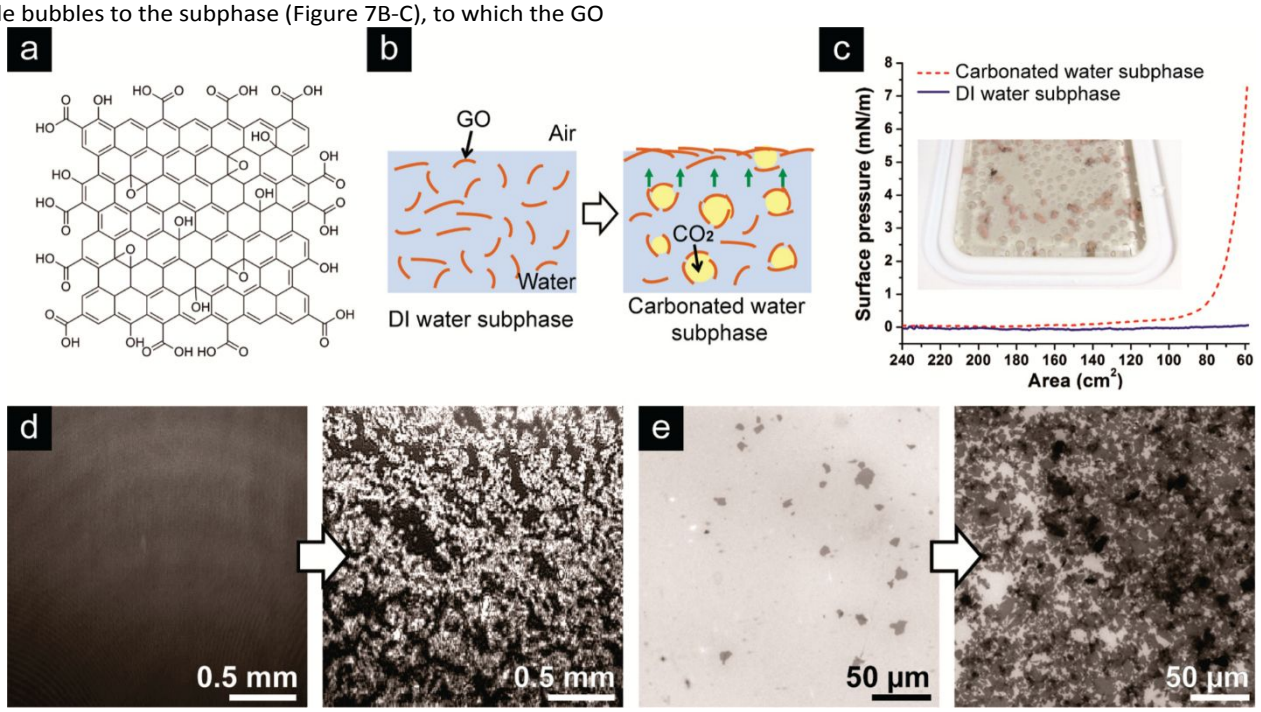

Figure 7. A) Possible chemical structure of graphene oxide (GO). B) Illustration showing the movement of GO flakes dissolved in the subphase to the air-water interface via carbon dioxide bubbles. C) Surface pressure over compression area measurements for GO on plain water (solid blue line) and on carbonated water subphase (dashed red line) demonstrated movement of GO flakes to the surface via carbon dioxide bubbles. Inset shows the flotation experiment in a Langmuir-Blodgett trough in which boiling stones were added to promote bubble evolution. D) *In situ* Brewster angle microscopy images of the air-water surface before (left) and after (right) GO flotation. E) Fluorescence quenching microscopy images of dip-coated substrates before (left) and after (right) GO flotation to the surface.[79] Reprinted with permission from ref [79]. Copyright 2010, American Chemical Society.

The variation in GO chemical structure makes interpreting results across experiments challenging. Computational efforts can assist by predicting likely structures iteratively. One report deployed *ab initio* MD simulations to consider the distribution of functional groups across GO.[80] Simulations under vacuum and water showed better thermal stability for molecules with semi-ordered distributions of hydroxide and epoxide groups, likely because clustering the functional groups reduced strain among the preserved graphene-like regions and promoted hydrogen bonding among oxygen-bearing functional groups. Another paper utilized *ab initio* MD simulations to consider water interactions with GO molecules with different carbon:oxygen ratios,[81] a common metric used to describe GO composition that can be experimentally measured. The GO sample with more oxygen groups, i.e. the oxidized GO, had more strongly hydrogen-bonded water molecules near the GO surface because it had more bonded water overall.

Interestingly, both of these MD papers also reported a dynamic chemical structure where GO interacts with surrounding water through its functional groups over time, including spontaneous epoxide opening (Figure 8A) and proton shuttling between surface hydroxide groups and water molecules (Figure 8B).[80, 81] The reactivity of GO in plain water was then investigated in detail via Born-Oppenheimer MD simulations.[82] GO sheets with two different carbon:oxygen ratios formed new species on the surface, including alkoxide, ether, and ketone groups. Epoxides on the GO may open to reduce strain and form carbocations with different lifetimes depending on the carbon:oxgen ratio of the GO. These carbocations could then interact with water to produce either an alcohol and hydronium for the oxidized GO or two alcohols for the reduced GO. Both GO structures could also protonate water via an existing alcohol. Overall, the oxidized GO facilitated and supported hydronium ion formation, which may shuttle protons around the GO surface and affect the chemical structure. The reduced GO did not form hydroniums as easily but could split water to form two new alcohol groups. The authors noted that reduced GO splitting water was a very rare event. The variation of GO chemical structure over time in simplistic environments is fascinating and requires additional,

detailed investigations. It is important to note these MD efforts only considered the effects of hydroxide and epoxide functional groups while GO is thought to have other groups. Additionally, GO flakes vary in size and functional group distributions, which may impact reactivity.

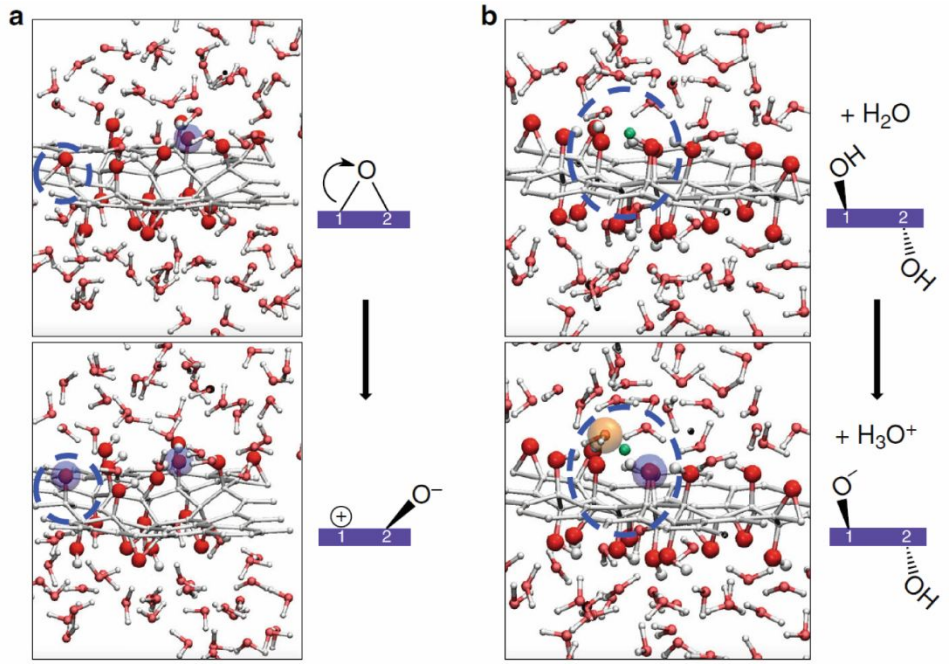

Figure 8. Molecular dynamic (MD) simulation snapshots along the trajectory of a semi-ordered graphene oxide (GO) model in water demonstrating chemical reactivity of GO. A) Epoxide opening mechanism. B) Deprotonation of a surface hydroxide to create a surface alcoholate (blue shaded circle) and an excess proton (orange shaded circle).[80] This figure has been reprinted from ref [80] under the terms of the Creative Commons CC BY 4.0 license.

Because GO is an amphiphile, it is interesting to consider if GO behaves like other amphiphiles including stabilizing surfactants.[83] While a detailed discussion of GO stability at other interfaces is beyond the scope of this review, it is worth noting that others have demonstrated stabilization of oil-water interfaces using GO[78] including spontaneous stabilization with additional surfactant molecules.[84, 85]

4.2 Water Organization: Structural Analyses

Structural information about GO organization at the air-water interface can be determined using liquid-surface XR. XR measurements of Langmuir GO films showed variation in reflectivity signal as the films at different film compressions, which were determined by the measured surface pressure (Figure 9A).[86] Data were fitted via the Parratt formalism to two unique slabs each with its own thickness, electron density, and roughness, which the authors interpreted as two layers of GO flakes on top of each other (Figure 9B-D). Additional grazing incidence X-ray diffraction measurements showed an out-of-plane diffraction peak, attributed to a layer of tilted GO flakes that stick out of the water surface. Recently, our group demonstrated a universal preparation method where commercial GO suspensions are sonicated in methanol, filtered to remove large (> 1.2 µm) aggregates, and then deposited on top of an aqueous subphase to create a high-quality, interfacial GO films.[87] It is important to note that because GO is water soluble, creating interfacial films is not trivial. The combination of sonicating and filtering reduced the necessary GO solution volume by 10 – 100x and helped to create significantly smoother films. XR analysis of GO solutions deposited using our preparation method showed distinct films at the air-water interface while untreated GO solutions did not create a cohesive structure. Analysis of commercially available GO solutions with different carbon:oxygen ratios additionally showed variation in film quality at the air-water interface depending on the specific GO used. Notably, the preparation of high-quality interfacial films facilitated liquid surface XR data collection up to Q = 0.7 Å^{-1}, which gives a vertical spatial resolution of 4.5 Å. In another work, we reproduced the best quality GO film on water.[1] XR data were fitted to 3 unique slabs at different distances from the air-water surface. The slab closest to the water had an electron density similar to water, 0.34 versus 0.33 e^-/Å^3 and a thickness of 19 Å, which we interpreted as an incomplete layer of submerged and tilted GO flakes. The next layer is closer to the air-water surface and has a much larger electron density of 0.50 e^-/Å^3 and a smaller thickness of 8.1 Å, both of which match hydrated GO. The last layer is slightly larger with a thickness of 11 Å and a much lower electron density of 0.04 e^-/Å^3. We interpreted this layer as the tops of tilted GO flakes sticking up out of the liquid surface, consistent with previous reports on bilayer GO formation.[86]

The thickness and electron densitiy values determined using liquid surface XR are also consistent with an NR study of GO films at the air-water inteface.[88] Interestingly, this NR study that compared GO film structures at the air-water interface for purified and unpurifed GO dispersions posited that oxidative debris affected film organization.[88] While oxidative debris generated during synthesis is certainly present in GO dispersions, it is difficult to determine if purification procedures remove this debris without also affecting GO flake structure and composition.

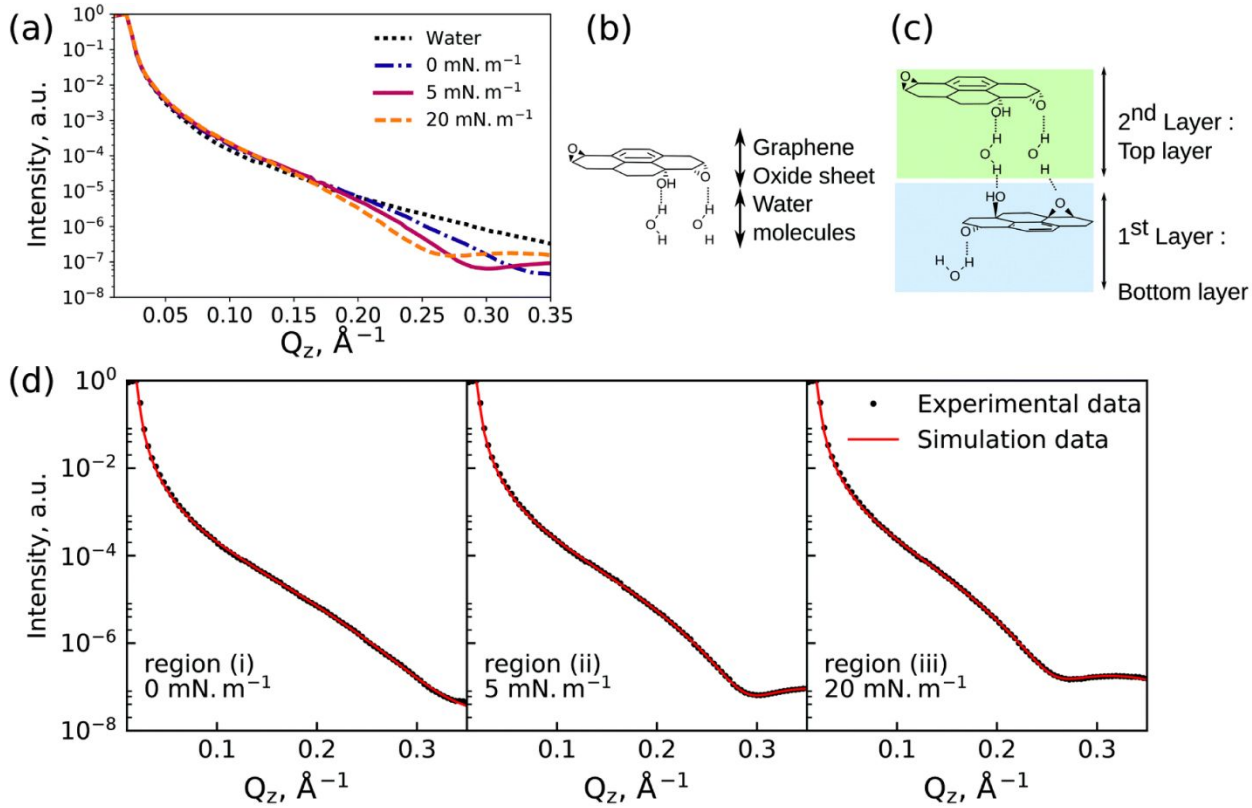

Figure 9. X-ray reflectivity intensity of pure water (black dotted line) and graphene oxide (GO) on water at 0 mN/m (blue dot dashed line), 5 mN/m (purple solid line), and 20 mN/m (yellow dashed line). B) Hydrated GO unit model used to fit reflectivity data. C) Proposed GO structure at the air-water interface. D) X-ray reflectivity intensities (black circles) and fits (red lines) at different surface pressures.[86] Figure reprinted from ref [86] with permission from the Royal Society of Chemistry, Copyright 2017.

Other works have studied GO films on solid substrates by contacting the samples with liquids. Reports focused on film hydration[89] and film "swelling" of organic solvents[90-93] found variation in the GO flake interlayer spacing as solvent molecules intercalate between GO flakes. Such behavior is driven by nanoscale interactions between the GO flakes and surrounding liquid but also affects macroscale GO properties. Therefore, multiscale investigations are necessary.

4.3 Water Organization: Chemical Analyses

Information about molecular water organization for GO at the air-water interface can be determined using SFG. Reports that considered water structure using SFG near GO films on solid substrates contacted with water showed significant contributions from the substrate hydroxyl groups,[81, 94] highlighting the importance of characterizing all components of the interface including substrate effects. Measurements of GO suspended directly on the air-water interface demonstrated two distinct water populations at ~3200 cm^{-1} and ~3400 cm^{-1}, attributed to strongly hydrogen-bonded and weakly hydrogen-bonded water, respectively.[94, 95] Additional measurements on high-quality GO films created with our preparation method revealed an additional peak around 3600 cm^{-1}, which we attributed to water trapped between the GO flakes[1, 87, 96] and was predicted via simulated SFG spectra previously.[81] This feature is distinct from the dangling hydroxide water stretch present at 3700 cm^{-1}, which has been observed for GO films with incomplete coverage due to water molecules at the bare air-water interface.[94] Variation of the water subphase pH at a fixed ionic strength revealed significant increases in the 3200 cm^{-1} and 3400 cm^{-1} bands for pH < 6, which we connected to the deprotonation of the carboxylic acid groups of the GO.[1] As the functional groups deprotonate, the magnitude of the GO surface charge increases, which induces water alignment and increases the overall SFG intensity. Similar results were obtained for subphases without a fixed ionic strength. From these changes in SFG intensity, we determined the pK_a of carboxylic acid groups on GO to be 4. This value is slightly acidic compared to bulk carboxylic acid titrations but consistent with other pK_a measurements of films at the air-water interface. It is

ARTICLE

important to note pK_a values can be different at interfaces because hydronium/hydroxide ions accumulate and affect protonation/deprotonation differently versus the bulk.

4.4 Ion Adsorption and Influence on Water Organization: Structural Analyses

The addition of ions complicates the interfacial behavior of GO, as ions may adsorb and affect GO flake distributions and water organization. GO has an intrinsic negative surface charge due to the deprotonation of functional groups present on its surface. Consequently, ions readily adsorb to GO films suspended at the air-water interface. Our group characterized ion adsorption to GO films prepared at the air-water interface using small flakes, ~0.2 nm in size.[95] XFNTR measurements revealed more trivalent ion adsorption compared to monovalent and divalent ion adsorption. Liquid surface XR showed multilayered GO films after trivalent ion adsorption while films composed on monovalent and divalent ion solutions were less distinct. GO films created using our universal preparation method also showed more trivalent ion adsorption for higher-quality films, meaning ion adsorption is facilitated by GO flake organization.[87] GO films with more oxygen functional groups per carbon-carbon bond, characterized using XPS, showed enhanced ion adsorption, as expected.

Because GO contains functional groups, the subphase pH plays an important role. Additionally, ion speciation in solution can vary over pH. In another work, we investigated the impact of pH on trivalent ion adsorption and GO film structure.[1] XFNTR data showed about 17x more trivalent ion adsorption for GO films on pH 9 subphases versus films on pH 3 subphase, attributed to an increase in the magnitude of the GO film charge until the pK_a of the carboxylic acid groups of GO is surpassed and to the adsorption of metal hydroxide species at very high pH. Liquid surface XR analysis showed excess electron density for GO films on high subphases, possibly from the additional atoms associated with the adsorbed metal hydroxide species. Notably, the subphase concentration was too low for visible precipitation, meaning the metal hydroxides may have nucleated on the GO film during adsorption.

To understand the impact of the ion character on sorption, we studied ion adsorption to GO films as a function of ion charge density and subphase concentration.[97] At low subphase concentrations, XFNTR analysis showed similar adsorption of ions with different charge densities to GO films at the air-water interface. Indeed, XR revealed nearly identical film structures. Remarkably, at high subphase concentrations, about 8x more of the higher charge density ions absorb versus the lower charge density ions. XR data reveal that most of the electron density, and subsequent XR signal, comes from the slabs closest to the liquid subphase. Although the GO film is multilayered, careful comparison to an ideal monolayer consisting of a carboxylic acid headgroup and a hydrocarbon tail revealed that significantly more higher charge density ions adsorb to the GO films than expected from a simple charge compensation.

4.5 Ion Adsorption and Influence on Water Organization: Chemical Analyses

Chemical information about water structuring near GO when ions are present can be obtained using SFG. Typically, SFG intensity in the water region decreases as ions adsorb, as these species will screen the surface charge of GO and disrupt local water organization near the interface. Indeed, the overall SFG intensity decreases for GO films transferred to a CaF2 prism (Figure 10A) and created directly on NaCl subphases as the salt concentration increases (Figure 10B-C).[94] Our group observed variation in SFG intensity for GO films for different alkali metal salts over subphase concentration where the SFG intensity increases until 100 μM and then decreases.[96] This variation was explained using the interference effect of SFG signal, where signals from different probe depths may destructively interfere thus decreasing the overall intensity, and changes in carboxylic acid group protonation from the addition of salts. Additionally, Li^+ showed different overall SFG signal, which was attributed to the retention of its hydration shell and inability to strongly interact with the aromatic rings of basal plane GO.

SFG intensity decreased as trivalent ions adsorb to GO films prepared with small flakes[95] and prepared with our universal preparation method.[87] Analysis of GO films on dilute trivalent ion subphases[1] with different pH values showed minimal signal for pH < 3, consistent with minimal ion adsorption revealed with XFNTR due to a minimal GO surface charge. The 3200 cm^{-1} and 3400 cm^{-1} band intensities increase for subphases between pH 3 and 7, where we also observed an increase in the surface charge magnitude due to carboxylic acid deprotonation and trivalent ion adsorption via XFNTR results. For pH > 7, the overall SFG signal increases substantially, which we attribute to adsorption of trivalent hydroxide complexes that can align water and possibly contribute to the SFG intensity. These results revealed a competition between an increase in the surface charge magnitude over increasing subphase pH, which should increase the SFG signal intensity, and an increase in the amount of adsorbed trivalent ion over increasing subphase pH, which should decrease the SFG signal intensity.

ARTICLE

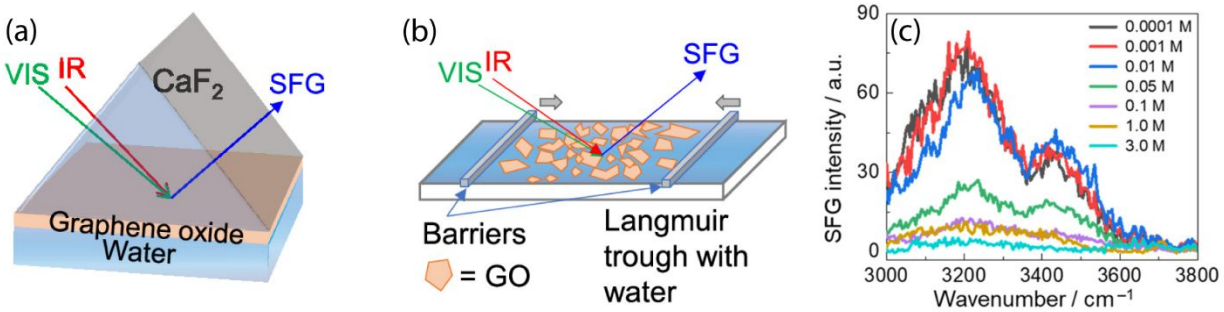

Figure 10. Vibrational sum frequency generation spectroscopy (SFG) setup using A) graphene oxide (GO) transferred onto a CaF_2 prism and contacted with water. B) SFG setup of free-standing GO at the air-water interface as prepared using a Langmuir trough. C) SFG intensity data of the hydroxide stretch region for GO on 0.0001 M (black), 0.001 M (red), 0.01 M (blue), 0.05 M (green), 0.1 M (purple), 1 M (yellow), and 3 M (cyan) NaCl subphases.[94] These figures have been adapted with permission from ref [94]. Copyright 2022 American Chemical Society.

Our group also considered the impact of trivalent ion charge density on water arrangement near interfacial GO films.[97] SFG analysis of GO films created on dilute subphases of higher and lower charge density ions showed similar 3200 cm^{-1} and 3400 cm^{-1} band intensities. SFG studies of GO films on high concentration subphases show a decrease in water signal, consistent with ion adsorption, for both trivalent ions. Interestingly, for the higher charge density ion, an additional red-shifted water peak appears, which we attribute to the dehydration of the adsorbed ions. This signal is more strongly present for fatty acid monolayers, composed of a carboxylic acid headgroup and a hydrocarbon tail, made on both high and low charge density ion subphases as well, indicating the adsorption is not necessarily unique to GO.

Electrochemistry measurements can provide indirect chemical information about electrode surfaces by measuring the total charge present near the system. Cyclic voltammetry (CV) measurements of GO deposited on glassy carbon electrodes in uranium solutions revealed small changes in the reduction/oxidation potentials of U(VI) to U(V)/U(V) to U(VI), attributed to differences in GO composition between the electrodes.[98] The authors speculated reduction occurs after adsorption. We note electrochemical impedance spectroscopy measurements of GO modified with different ILs revealed variations in cation and anion diffusion through GO membranes made from stacked GO flakes, which was connected to changes in the hydrophobicity of the GO.[99] Additional simulations showed an increase in water diffusion across GO depending on the IL used during GO modification.

SCM investigations of ion adsorption to GO can provide some plausible surface explanations for trends observed with bulk techniques. A report considered U(VI) and Eu(III) ion adsorption to GO as a function of pH and ion concentration.[100] Acid-base titration data of GO dispersions revealed two pK_a values, attributed to the deprotonation of carboxylic acid and sulfonate groups present on the GO, the latter of which is thought to be an impurity introduced during synthesis. SCM trials were validated with these titration data and then used to model batch adsorption. The results showed U(VI) preferentially adsorbs to the carboxylic acid groups of GO for all pH values while Eu(III) may adsorb to the sulfonate groups at low pH. Another work by the same group considered Th(IV) and Np(V) adsorption with bath sorption data and SCM (Figure 11A).[101] Modelling showed a decrease in Th(IV) adsorption, attributed to the competition of adsorption to GO and Th(IV) hydrolysis. Generally, Th(IV) adsorbed to the present carboxylic acid groups while Np(V) only adsorbed to the sulfonate groups. The authors compared the SCM-derived equilibria constants for ion complexation to carboxylate groups on the GO to equilibria constants for ion complexation to carbonates in solution and found a linear relationship across ion oxidation state (Figure 11B). This linearity implies ion coordination to GO strongly depends on the ion oxidation state where ions with the larger effective charges adsorb to GO more than ions with smaller effective charges. Notably, these works highlight the importance of considering impurities in samples, as some ions may preferentially interact with contaminates thus impacting overall adsorption.

The structure and composition of the GO impacts ion adsorption. The introduction of defects to GO flakes during synthesis improved U(VI) and Am(III) adsorption.[102] SCM models of batch ion sorption data showed ions primarily interact with the carboxylic acid groups present on GO. XPS analysis revealed more carboxylic groups were present for the defective GO, which the authors speculate is because defective GO contains more holes and carboxylic acid groups primarily exist along GO edges. X-ray absorption spectroscopy showed similar U(VI) interactions with both typical and defective GO, meaning the adsorption mechanism is not affected by the introduction of holes and defects. Another work combined X-

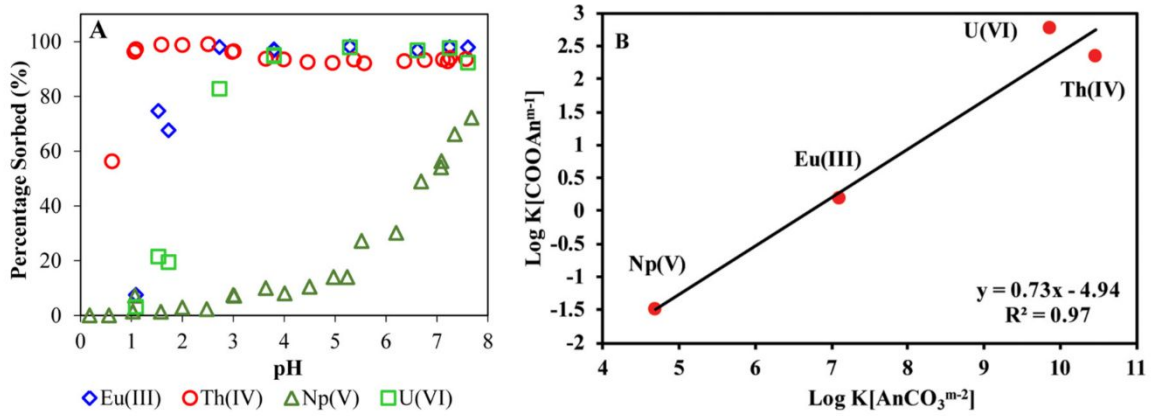

Figure 11. A) Experimentally measured ion adsorption of Eu(III) (blue diamonds), Th(IV) (red circles), Np(V) (dark green triangles), and U(VI) (light green squares) to graphene oxide (GO) as a functional of bulk pH. B) Equilibria constant comparison of ion complexation to carboxylate groups of GO plotted over ion complexation to carbonates in bulk liquid.[101] This figure has been reprinted with permission from ref [101]. Copyright American Chemical Society, 2018.

Interestingly, ions may adsorb to GO without necessarily interacting with the functional groups of GO. Reduced GO contains fewer functional groups compared to typical GO and has been shown to reduce solution gold to metallic gold via its more graphene-like regions.[106] SEM and XPS analysis confirmed metallic gold nanoparticle formation after adsorption and comparisons of extraction efficiency for different GOs, graphene, and graphite as well as extractions at different temperatures showed that the graphene-like regions of reduced GO can donate electrons and reduce solution $AuCl_4^-$ to Au^0, which then on the reduced GO surface. The authors demonstrated possible gold extraction in very dilute limits, simulated sea water, and acidic electronic wastes.

4.6 Ion Adsorption and Water Behaviour in Three-Dimensional Graphene Oxide Samples

Lastly, we note the importance of considering interfacial water and ion structure near GO for effective and efficient three-dimensional GO applications, such as GO membrane fabrication and GO sorption. Recently, our group connected detailed interfacial structural and chemical analysis to GO membrane performance, which is usually assessed using bulk techniques.[1] Full reviews of GO membrane fabrication and performance can be found elsewhere.[107-109] Briefly, GO membranes usually consist of stacked GO flakes on a support substrates. Additional ions, molecules, and polymers may be included to manipulate the interlayer GO flake distance, which can allow ion sieving via size exclusion. Indeed, works have demonstrated impressive ion separations using GO membranes.[110, 111] Another work demonstrated three-dimensional GO structures with impressive ion sorptions.[112] However, little information has been provided about the exact ray absorption spectroscopy and DFT calculations to understand variation in U(VI) and Am(III)/Eu(III) adsorption to GOs with different carbon:oxygen ratios, which was linked to the number of carboxylic acid groups present.[103] A recent *ab initio* MD simulation on organic molecular aniline adsorption to GO, observed preferential hydrogen bond formation between the epoxide groups of GO and the aniline.[104] These observations point toward the important role of carboxylic acids in ion interactions with GO. However, the influences of other functional groups cannot be ignored and may play a significant role for ions and molecules. For example, one report demonstrated divalent ion adsorption to a GO synthesized with significantly fewer carboxylic acid groups.[105]

5. Perspectives and Outlooks

Given the importance of graphene and GO in applications spanning from catalysis to tribology to separations, it is critical to comprehend molecular-scale chemical and structural information about the interfaces formed between these materials and liquid water. The current major challenges of the field include: 1) creation of reproducible, high-quality graphene and GO surfaces with minimized substrate effects; 2) direct observation of water orientation and structure near graphene and GO both in water and with ions present; 3) determining the chemical structure and reactivity of GO in water; and 4) systematic control of functional group types, location, and density on GO.

As discussed previously, obtaining high-quality graphene and GO surfaces is not trivial, as typical preparations require multiple steps where water and ions may be introduced. Airborne hydrocarbons may also deposit on clean sample surfaces and alter observed structures. Evidently, researchers should strive to create reproducible graphene and GO surfaces and articles should report full and comprehensive sample preparations with complete structural and chemical characterizations. Cleaning procedures and measurements under inert atmospheres offer additional strategies to understand and possibly control contamination. Similarly, the role of the chosen substrate in the graphene and GO system should be examined critically. Given the demonstrated variation in macroscale properties of graphene as induced by different substrates, nanoscale organizations and structures must also be affected. Considering graphene and GO on different substrates

and performing control measurements of the substrate alone can provide reasonable comparisons.

With these higher-quality, reproducible surfaces comes the opportunity to directly examine and understand interfacial water near graphene and GO. Extensive computational studies have suggested enhanced water orientation near graphene yet comparable experimental studies are lacking. Both chemical and structural probes sensitive to water should be utilized to directly examine water behavior in pure liquid and solutions containing ions. Probing these systems as a function of solution conditions and graphene/GO properties will yield critical fundamental information that strongly impacts the success of downstream applications.

Given the large variation in GO syntheses, which create different chemical and physical structures and properties, it is necessary to determine the stability of GO in simple liquids including pure water. Excellent simulation studies have shown that GO may react with water via simple protonation/deprotonation and more complex chemical bond rearrangement. To date, no experiments have directly observed this reactivity despite numerous GO publications. Direct spectroscopic studies on well-prepared samples are critical for understanding such reactivity.

The controlled synthesis of GO with deliberate functional group placement and manipulation has been a goal in GO synthesis for decades and there have been great strides toward tuning GO properties. Additional success across the field necessitates reporting complete chemical and structural analyses of prepared GO with particular attention paid toward the variation in properties of bulk and surface samples.

Additionally, there exists a substantial gap between computational and experimental studies. Classical and *ab initio* MD are powerful techniques that enable direct examination of targeted surfaces, water, and, if present, ions. Comparison to experimental data can be especially fruitful but requires effort from both communities to allow meaningful interpretation. Typical simulation works consider small simplistic surfaces with high ion concentrations and require a predetermined equilibration time. Experimental observations are usually averaged over a real surface, where defects are likely present, under presumable equilibria conditions unless otherwise stated. Careful control experiments are necessary to ground simulations and examination of accessible concentrations and surfaces is critical for allowing reasonable overlap.

6. Conclusions

The organization of water and ions near graphene and GO is both fundamentally interesting and technologically relevant. Probing these interactions requires a comprehensive physical and chemical description of the interface formed between the graphene or GO and the surrounding media, usually water or air. Understanding the fundamental properties of water and ion structure near these two-dimensional materials requires robust and complete descriptions of the interface, including water organization and orientation, ion adsorption, and the structure and chemistry of the surface itself. Both substrate and contamination effects must also be considered. We presented an overview of recent works completed on water and ion behavior near graphene and GO with a particular emphasis on structural and chemical characterization and interfacial specificity. The major findings include:

I. Water forms 1-3 hydration layers near plain graphene with and without an applied potential, as determined with experimental structural techniques and computer simulations. Additional efforts are needed to experimentally probe molecular water orientation, as current studies have observed significant substrate and contamination effects.

II. Ions may adsorb to plain graphene under an applied potential electrostatically. To date, a clear chemical interpretation of water arrangement and ion organization near graphene is lacking. Previous works have shown the challenges associated with creating reproducible, clean graphene samples and deconvoluting water and ion signals.

III. GO is not a single molecule with a predetermined chemical structure. Rather, GO is a family of molecules containing sp^2 aromatic carbon regions and oxygen functional groups. Works have demonstrated GO amphiphile behavior, including isolation at air-water interfaces. Computational works have suggested a reactive chemical structure that varies as GO flakes contact air and water. Experimental observation of these chemical structure changes, especially for different GO flake compositions and over time as well as the impact of this intrinsic reactivity on water and ion organization, are thus necessary.

IV. Water readily exists near GO at interfaces, as determined using chemically sensitive techniques, and may intercalate in between stacked GO flakes. Because GO has an intrinsic surface charge, ions may adsorb and interact with the functional groups present on GO, of which carboxylic acid has received considerable attention. Future directions should include systematically unravelling the impact of GO flake structure and functional group placement on adsorption. Lastly, water and ion behaviors near GO are especially relevant for downstream application efforts.

These summary points and suggestions for future works will considerably advance our understanding of these complex graphene and GO interfaces and ultimately pave the way toward useful downstream applications.

Author Contributions

The manuscript was written using contributions of all authors. All authors have given approval to the final version of the manuscript.

Conflicts of interest

The authors declare no conflicts of interest.

Acknowledgements

This material is based upon work supported by the U.S. Department of Energy, Office of Basic Energy Science, Division of Chemical Sciences, Geosciences, and Biosciences, Early Career Research Program under Contract DE-AC02-06CH11357.

References

1. A. J. Carr, S. E. Lee, R. R. Kumal, W. Bu and A. Uysal, *ACS Appl. Mater. Interfaces*, 2022, **14**, 57133-57143.
2. A. J. Carr, S. S. Lee and A. Uysal, *J. Phys.: Condens. Matter*, 2022, **34**, 144001.
3. A. Gutiérrez-Cruz, A. R. Ruiz-Hernández, J. F. Vega-Clemente, D. G. Luna-Gazcón and J. Campos-Delgado, *J. Mater. Sci.*, 2022, **57**, 14543-14578.
4. W. T. Tee, N. Y. L. Loh, K. C. Lai, B. Y. Z. Hiew, S. Gan and L. Y. Lee, *Sep. Purif. Technol.*, 2023, **320**.
5. K. Pal, A. Si, G. S. El-Sayyad, M. A. Elkodous, R. Kumar, A. I. El-Batal, S. Kralj and S. Thomas, *Crit. Rev. Solid State Mater. Sci.*, 2020, **46**, 385-449.
6. S. Bagyalakshmi, A. Sivakami, K. Pal, R. Sarankumar and C. Mahendran, *J. Nanopart. Res.*, 2022, **24**.
7. K. Pal, N. Asthana, A. A. Aljabali, S. K. Bhardwaj, S. Kralj, A. Penkova, S. Thomas, T. Zaheer and F. Gomes de Souza, *Crit. Rev. Solid State Mater. Sci.*, 2021, **47**, 691-707.
8. N. Nath, A. Kumar, S. Chakroborty, S. Soren, A. Barik, K. Pal and F. G. de Souza, Jr., *ACS Omega*, 2023, **8**, 4436-4452.
9. K. Pal, S. Chakroborty, P. Panda, N. Nath and S. Soren, *Environ. Sci. Pollut. Res. Int.*, 2022, **29**, 76626-76643.
10. O. M. Ama, U. O. Aigbe, W. W. Anku, O. A. Osibote and K. Pal, *Top. Catal.*, 2022, **65**, 1745-1754.
11. A. Si, G. Z. Kyzas, K. Pal and F. G. de Souza Jr, *J. Mol. Struct.*, 2021, **1239**.
12. L. Fumagalli, A. Esfandiar, R. Fabregas, S. Hu, P. Ares, A. Janardanan, Q. Yang, B. Radha, T. Taniguchi, K. Watanabe, G. Gomila, K. S. Novoselov and A. K. Geim, *Science*, 2018, **360**, 1339-1342.
13. M. H. Motevaselian and N. R. Aluru, *ACS Nano*, 2020, **14**, 12761-12770.
14. S. Varghese, S. K. Kannam, J. S. Hansen and P. S. S, *Langmuir*, 2019, **35**, 8159-8166.
15. J. Olivieri, J. Hynes and D. Laage, *J. Phys. Chem. Lett.*, 2021, **12**, 4319-4326.
16. A. J. Grooms, J. F. Neal, K. C. Ng, W. Zhao, A. H. Flood and H. C. Allen, *J. Phys. Chem. A*, 2020, **124**, 5621-5630.
17. P. A. Fenter, *Rev. Mineral. Geochem.*, 2002, **49**, 149-221.
18. M. K. Bera, W. Bu and A. Uysal, in *Physical Chemistry of Gas-Liquid Interfaces*, eds. J. Faust and J. House, Elsevier, 2018, pp. 167-194.
19. P. S. Pershan and M. Schlossman, *Liquid surfaces and interfaces: synchrotron x-ray methods*, Cambridge University Press, 2012.
20. M. Tolan, *X-ray scattering from soft-matter thin films*, Springer Berlin, Heidelberg, 1999.
21. H. Zabel, *Appl. Phys. A*, 1994, **58**, 159-168.
22. C. Park and P. A. Fenter, *J. Appl. Crystallogr.*, 2007, **40**, 290-301.
23. A. J. Carr, *Nat. Rev. Phys.*, 2022, **4**, 743-743.
24. P. Sun, E. A. Binter, Z. Liang, M. A. Brown, A. V. Gelis, I. Benjamin, M. K. Bera, B. Lin, W. Bu and M. L. Schlossman, *ACS Cent. Sci.*, 2021, **7**, 1908-1918.
25. S. Yoo, B. Qiao, T. Douglas, W. Bu, M. Olvera de la Cruz and P. Dutta, *ACS Appl. Mater. Interfaces*, 2022, **14**, 7504-7512.
26. W. Bu, M. Mihaylov, D. Amoanu, B. Lin, M. Meron, I. Kuzmenko, L. Soderholm and M. L. Schlossman, *J. Phys. Chem. B*, 2014, **118**, 12486-12500.
27. J. M. Yuk, J. Park, P. Ercius, K. Kim, D. J. Hellebusch, M. F. Crommie, J. Y. Lee, A. Zettl and A. P. Alivisatos, *Science*, 2012, **336**, 61-64.
28. R. Garcia, *ACS Nano*, 2023, **17**, 51-69.
29. A. Maestro and P. Gutfreund, *Adv. Colloid Interface Sci.*, 2021, **293**, 102434.
30. M. Bonn, Y. Nagata and E. H. Backus, *Angew. Chem. Int. Ed.*, 2015, **54**, 5560-5576.
31. C. M. Johnson and S. Baldelli, *Chem. Rev.*, 2014, **114**, 8416-8446.
32. P. E. Ohno, H. F. Wang and F. M. Geiger, *Nat. Commun.*, 2017, **8**, 1032.
33. H. Zhou, P. Ganesh, V. Presser, M. C. F. Wander, P. Fenter, P. R. C. Kent, D.-e. Jiang, A. A. Chialvo, J. McDonough, K. L. Shuford and Y. Gogotsi, *Phys. Rev. B*, 2012, **85**.
34. F. Jiménez-Ángeles, K. J. Harmon, T. D. Nguyen, P. Fenter and M. Olvera de la Cruz, *Phys. Rev. Res.*, 2020, **2**, 043244.
35. N. Naguib, H. Ye, Y. Gogotsi, A. G. Yazicioglu, C. M. Megaridis and M. Yoshimura, *Nano Lett.*, 2004, **4**, 2237-2243.
36. G. Algara-Siller, O. Lehtinen, F. C. Wang, R. R. Nair, U. Kaiser, H. A. Wu, A. K. Geim and I. V. Grigorieva, *Nature*, 2015, **519**, 443-445.
37. J. Peng, J. Guo, R. Ma and Y. Jiang, *Surf. Sci. Rep.*, 2022, **77**.
38. M. R. Uhlig and R. Garcia, *Nano Lett.*, 2021, **21**, 5593-5598.
39. S. Singla, E. Anim-Danso, A. E. Islam, Y. Ngo, S. S. Kim, R. R. Naik and A. Dhinojwala, *ACS Nano*, 2017, **11**, 4899-4906.
40. A. Montenegro, C. Dutta, M. Mammetkuliev, H. Shi, B. Hou, D. Bhattacharyya, B. Zhao, S. Cronin and A. Benderskii, *Nature*, 2021, **594**, 62-+.
41. S. Nihonyanagi, S. Yamaguchi and T. Tahara, *J. Chem. Phys.*, 2009, **130**, 204704.
42. Y.-C. Wen, S. Zha, X. Liu, S. Yang, P. Guo, G. Shi, H. Fang, Y. R. Shen and C. Tian, *Phys. Rev. Lett.*, 2016, **116**, 016101.
43. I. V. Stiopkin, C. Weeraman, P. A. Pieniazek, F. Y. Shalhout, J. L. Skinner and A. V. Benderskii, *Nature*, 2011, **474**, 192-195.
44. Y. Zhang, H. B. de Aguiar, J. T. Hynes and D. Laage, *J. Phys. Chem. Lett.*, 2020, **11**, 624-631.
45. A. Montenegro, A. E. Vaughn, M. Mammetkuliyev, B. Zhao, B. Zhang, H. Shi, D. Bhattacharyya, A. V. Benderskii and S. B. Cronin, *J. Phys. Chem. C*, 2022, **126**, 20831-20839.
46. Y. Wang, T. Seki, X. Yu, C. C. Yu, K. Y. Chiang, K. F. Domke, J. Hunger, Y. Chen, Y. Nagata and M. Bonn, *Nature*, 2023, **615**, E1-E2.
47. Y. Wang, T. Seki, X. Liu, X. Yu, C. C. Yu, K. F. Domke, J. Hunger, M. T. M. Koper, Y. Chen, Y. Nagata and M. Bonn, *Angew. Chem.*, 2023, **62**, e202216604.
48. L. B. Dreier, Z. Liu, A. Narita, M. J. van Zadel, K. Mullen, K. J. Tielrooij, E. H. G. Backus and M. Bonn, *J. Phys. Chem. C*, 2019, **123**, 24031-24038.

49. D. Kim, E. Kim, S. Park, S. Kim, B. K. Min, H. J. Yoon, K. Kwak and M. Cho, *Chem*, 2021, **7**, 1602-1614.
50. E. Kim, D. Kim, K. Kwak, Y. Nagata, M. Bonn and M. Cho, *Chem*, 2022, **8**, 1187-1200.
51. C. Melios, C. E. Giusca, V. Panchal and O. Kazakova, *2D Mater.*, 2018, **5**.
52. D. M. Goggin, R. H. Bei, R. Anderson, D. A. Gomez-Gualdron and J. R. Samaniuk, *J. Phys. Chem. C*, 2021, **125**, 7880-7888.
53. D. M. Goggin and J. R. Samaniuk, *AIChE J.*, 2018, **64**, 3177-3187.
54. D. M. Goggin and J. R. Samaniuk, *Langmuir*, 2021, **37**, 14157-14166.
55. D. M. Goggin, H. Zhang, E. M. Miller and J. R. Samaniuk, *ACS Nano*, 2020, **14**, 777-790.
56. F. Jiménez-Ángeles and M. Lozada-Cassou, *J. Phys. Chem. B*, 2004, **108**, 7286-7296.
57. M. J. Bedzyk, G. M. Bommarito, M. Caffrey and T. L. Penner, *Science*, 1990, **248**, 52-56.
58. A. A. Chialvo and J. M. Simonson, *Condens. Matter Phys.*, 2011, **14**.
59. L. Zhou, L. Islas, N. Taylor, O. Bikondoa, E. Robles and W. H. Briscoe, *Carbon*, 2019, **143**, 97-105.
60. Y. Song, W. Zou, Q. Lu, L. Lin and Z. Liu, *Small*, 2021, **17**, e2007600.
61. D. L. McCaffrey, S. C. Nguyen, S. J. Cox, H. Weller, A. P. Alivisatos, P. L. Geissler and R. J. Saykally, *Proc. Natl. Acad. Sci. U.S.A.*, 2017, **114**, 13369-13373.
62. S. Yang, X. Zhao, Y. H. Lu, E. S. Barnard, P. Yang, A. Baskin, J. W. Lawson, D. Prendergast and M. Salmeron, *J. Am. Chem. Soc.*, 2022, **144**, 13327-13333.
63. W. M. de Vos and S. Lindhoud, *Adv. Colloid Interface Sci.*, 2019, **274**, 102040.
64. E. Gonzalez-Tovar and M. Lozada-Cassou, *Adv. Colloid Interface Sci.*, 2019, **270**, 54-72.
65. C. Y. Son and Z. G. Wang, *Proc. Natl. Acad. Sci. U.S.A.*, 2021, **118**.
66. Y. L. Wang, B. Li, S. Sarman, F. Mocci, Z. Y. Lu, J. Yuan, A. Laaksonen and M. D. Fayer, *Chem. Rev.*, 2020, **120**, 5798-5877.
67. H. Zhou, M. Rouha, G. Feng, S. S. Lee, H. Docherty, P. Fenter, P. T. Cummings, P. F. Fulvio, S. Dai, J. McDonough, V. Presser and Y. Gogotsi, *ACS Nano*, 2012, **6**, 9818-9827.
68. A. Uysal, H. Zhou, G. Feng, S. S. Lee, S. Li, P. Fenter, P. T. Cummings, P. F. Fulvio, S. Dai, J. K. McDonough and Y. Gogotsi, *J. Phys. Chem. C*, 2014, **118**, 569-574.
69. L. A. Jurado and R. M. Espinosa-Marzal, *Sci. Rep.*, 2017, **7**, 4225.
70. A. Uysal, H. Zhou, G. Feng, S. S. Lee, S. Li, P. T. Cummings, P. F. Fulvio, S. Dai, J. K. McDonough, Y. Gogotsi and P. Fenter, *J. Phys.: Condens. Matter*, 2015, **27**, 032101.
71. B. Demir and D. J. Searles, *Nanomaterials*, 2020, **10**, 2181.
72. C. Noh and Y. Jung, *Phys. Chem. Chem. Phys.*, 2019, **21**, 6790-6800.
73. S. Begić, F. Chen, E. Jónsson and M. Forsyth, *Phys. Rev. Mater.*, 2019, **3**, 095801.
74. S. Guo, S. Garaj, A. Bianco and C. Ménard-Moyon, *Nat. Rev. Phys.*, 2022, **4**, 247-262.
75. D. Lopez-Diaz, M. D. Merchan and M. M. Velazquez, *Adv. Colloid Interface Sci.*, 2020, **286**, 102312.
76. K. Z. Donato, H. L. Tan, V. S. Marangoni, M. V. S. Martins, P. R. Ng, M. C. F. Costa, P. Jain, S. J. Lee, G. K. W. Koon, R. K. Donato and A. H. Castro Neto, *Sci. Rep.*, 2023, **13**, 6064.
77. L. J. Cote, F. Kim and J. Huang, *J. Am. Chem. Soc.*, 2009, **131**, 1043-1049.
78. J. Kim, L. J. Cote, F. Kim, W. Yuan, K. R. Shull and J. Huang, *J. Am. Chem. Soc.*, 2010, **132**, 8180-8186.
79. F. Kim, L. J. Cote and J. Huang, *Adv. Mater.*, 2010, **22**, 1954-1958.
80. F. Mouhat, F.-X. Coudert and M.-L. Bocquet, *Nat. Commun.*, 2020, **11**, 1566.
81. R. David, A. Tuladhar, L. Zhang, C. Arges and R. Kumar, *J. Phys. Chem. B*, 2020, **124**, 8167-8178.
82. R. David and R. Kumar, *Chem. Commun.*, 2021, **57**, 11697-11700.
83. T. M. McCoy, G. Turpin, B. M. Teo and R. F. Tabor, *Curr. Opin. Colloid Interface Sci.*, 2019, **39**, 98-109.
84. G. A. Turpin, S. A. Holt, J. M. P. Scofield, B. M. Teo and R. F. Tabor, *Adv. Mater. Interfaces*, 2020, **7**, 1901810.
85. T. M. McCoy, A. J. Armstrong, J. E. Moore, S. A. Holt, R. F. Tabor and A. F. Routh, *Phys. Chem. Chem. Phys.*, 2022, **24**, 797-806.
86. N. Bonatout, F. Muller, P. Fontaine, I. Gascon, O. Konovalov and M. Goldmann, *Nanoscale*, 2017, **9**, 12543-12548.
87. R. Kumal, A. J. Carr and A. Uysal, *Chemrxiv*, 2022, 10.26434/chemrxiv-22022-26431csxr.
88. D. Lopez-Diaz, M. D. Merchan, M. M. Velazquez and A. Maestro, *ACS Appl. Mater. Interfaces*, 2020, **12**, 25453-25463.
89. A. Iakunkov and A. V. Talyzin, *Nanoscale*, 2020, **12**, 21060-21093.
90. A. Klechikov, J. Sun, A. Vorobiev and A. V. Talyzin, *J. Phys. Chem. C*, 2018, **122**, 13106-13116.
91. A. Iakunkov, J. Sun, A. Rebrikova, M. Korobov, A. Klechikov, A. Vorobiev, N. Boulanger and A. V. Talyzin, *J. Mater. Chem. A*, 2019, **7**, 11331-11337.
92. H. Lin, A. Iakunkov, N. Severin, A. V. Talyzin and J. P. Rabe, *J. Phys. Chem. C*, 2022, **126**, 20658-20667.
93. A. Iakunkov, N. Boulanger, A. Nordenström and A. V. Talyzin, *Adv. Mater. Interfaces*, 2021, **8**.
94. Y. Hong, J. He, C. Zhang and X. Wang, *J. Phys. Chem. C*, 2022, **126**, 1471-1480.
95. A. J. Carr, R. R. Kumal, W. Bu and A. Uysal, *Carbon*, 2022, **195**, 131-140.
96. S. E. Lee, A. J. Carr, R. R. Kumal and A. Uysal, *ChemRxiv*, 2023, 10.26434/chemrxiv-22023-dj26434m26430-v26432.
97. A. J. Carr, S. E. Lee and A. Uysal, *J. Phys. Chem. C*, 2023, **127**, 14363-14373.
98. V. N. Bliznyuk, N. A. Conroy, Y. Xie, R. Podila, A. M. Rao and B. A. Powell, *Phys. Chem. Chem. Phys.*, 2018, **20**, 1752-1760.
99. S. Tan, D. Zhang, M. T. Nguyen, V. Shutthanandan, T. Varga, R. Rousseau, G. E. Johnson, V. A. Glezakou and V. Prabhakaran, *ACS Appl. Mater. Interfaces*, 2022, **14**, 19031-19042.
100. Y. Xie, E. M. Helvenston, L. C. Shuller-Nickles and B. A. Powell, *Environ. Sci. Technol.*, 2016, **50**, 1821-1827.
101. Y. Xie and B. A. Powell, *ACS Appl. Mater. Interfaces*, 2018, **10**, 32086-32092.
102. N. Boulanger, A. S. Kuzenkova, A. Iakunkov, A. Y. Romanchuk, A. L. Trigub, A. V. Egorov, S. Bauters, L. Amidani, M. Retegan, K. O. Kvashnina, S. N. Kalmykov and A. V. Talyzin, *ACS Appl. Mater. Interfaces*, 2020, **12**, 45122-45135.

103. A. S. Kuzenkova, A. Y. Romanchuk, A. L. Trigub, K. I. Maslakov, A. V. Egorov, L. Amidani, C. Kittrell, K. O. Kvashnina, J. M. Tour, A. V. Talyzin and S. N. Kalmykov, *Carbon*, 2020, **158**, 291-302.
104. V. Subasinghege Don, L. Kim, R. David, J. A. Nauman and R. Kumar, *J. Phys. Chem. C*, 2023, **127**, 5920-5930.
105. J. Shayimova, R. R. Amirov, A. Iakunkov, A. Talyzin and A. M. Dimiev, *Phys. Chem. Chem. Phys.*, 2021, **23**, 17430-17439.
106. F. Li, J. Zhu, P. Sun, M. Zhang, Z. Li, D. Xu, X. Gong, X. Zou, A. K. Geim, Y. Su and H. M. Cheng, *Nat. Commun.*, 2022, **13**, 4472.
107. F. Jia, X. Xiao, A. Nashalian, S. Shen, L. Yang, Z. Han, H. Qu, T. Wang, Z. Ye, Z. Zhu, L. Huang, Y. Wang, J. Tang and J. Chen, *Nano Res.*, 2022, **15**, 6636-6654.
108. L. Yang, X. Xiao, S. Shen, J. Lama, M. Hu, F. Jia, Z. Han, H. Qu, L. Huang, Y. Wang, T. Wang, Z. Ye, Z. Zhu, J. Tang and J. Chen, *ACS Appl. Nano Mater.*, 2022, **5**, 3121-3145.
109. M. Aizudin, N. H. Alias, Y. X. A. Ng, M. H. Mahmod Fadzuli, S. C. Ang, Y. X. Ng, R. Poolamuri Pottammel, F. Yang and E. H. Ang, *Nanoscale*, 2022, **14**, 17871-17886.
110. Z. Wang, L. Huang, X. Dong, T. Wu, Q. Qing, J. Chen, Y. Lu and C. Xu, *Nat. Commun.*, 2023, **14**, 261.
111. P. K. Narayanam, S. Sriram and K. Sundararajan, *J. Water Process Eng.*, 2020, **38**.
112. N. Boulanger, A. S. Kuzenkova, A. Iakunkov, A. Nordenstrom, A. Y. Romanchuk, A. L. Trigub, P. V. Zasimov, M. Prodana, M. Enachescu, S. Bauters, L. Amidani, K. O. Kvashnina, S. N. Kalmykov and A. V. Talyzin, *Adv. Mater. Interfaces*, 2022, **9**.